THE JOURNAL OF BIOLOGICAL CHEMISTRY VOL. 281, NO. 10, pp. 6643–6650, March 10, 2006

Probing the Functional Link between Androgen Receptor Coactivator and Ligand-binding Sites in Prostate Cancer and Androgen Insensitivity*

Received for publication, October 31, 2005, and in revised form, December 16, 2005 Published, JBC Papers in Press, December 19, 2005, DOI 10.1074/jbc.M511738200

Bin He[‡1], Robert T. Gampe, Jr.[§], Andrew T. Hnat[‡], Jonathan L. Faggart[‡], John T. Minges[‡], Frank S. French[‡], and Elizabeth M. Wilson[‡2]

From the [‡]Laboratories for Reproductive Biology, Lineberger Comprehensive Cancer Center, Department of Pediatrics, Biochemistry and Biophysics, University of North Carolina, Chapel Hill, North Carolina 27599 and [§]Discovery Research, GlaxoSmithKline, Research Triangle Park, North Carolina 27709

The androgen receptor (AR) is a ligand-activated transcription factor required for male sex development and virilization and contributes to prostate cancer initiation and progression. High affinity androgen binding triggers conformational changes required for AR transactivation. Here we characterized naturally occurring AR gene mutations in the region of activation function 2 (AF2) that decrease or increase AR transcriptional activity by altering the region bounded by AF2 and the ligand binding pocket without affecting equilibrium androgen binding affinity. In the androgen insensitivity syndrome, germ line AR mutations increase the androgen dissociation rate and reduce AR F*XX*LF motif binding and the recruitment of steroid receptor coactivator (SRC)/p160 coactivator L*XX*LL motifs. In prostate cancer, somatic AR mutations in AF2 or near the bound ligand slow androgen dissociation and increase AR stabilization and coactivator recruitment. Crystal structures of the AR ligand binding domain bound to R1881 and F*XX*LF or L*XX*LL motif peptide indicate the mutations are proximal to the AF2 bound peptide, adjacent to the ligand pocket, or in a putative ligand gateway. The results suggest a bidirectional structural relay between bound ligand and coactivator that establishes AR functional potency *in vivo*.

Steroid receptors comprise a subgroup of the nuclear receptor family of transcriptional activators that regulate gene expression by recruiting coactivator proteins (1). Like other steroid receptors, the androgen receptor (AR)[3] mediates transcriptional activation primarily through two domains. Activation function 1 (AF1) in the NH_2-terminal region is the major transactivation domain (2) but is not well conserved across species (3). Activation function 2 (AF2) in the ligand binding domain is a highly conserved hydrophobic surface that is stabilized by agonist binding and required for SRC/p160 coactivator recruitment. AF2 is formed by helices 3, 3′, 4, and 12 and is flanked by clusters of oppositely charged residues (4). AR binding of the biologically active androgens testosterone and dihydrotestosterone (DHT) is thought to stabilize the AF2 helix 12 to complete the coactivator binding surface (5–7).

The human AR gene is expressed at chromosome Xq11-12 as a single allele in the 46,XY genetic male. More than 300 different AR single amino acid mutations or partial gene deletions cause the androgen insensitivity syndrome (AIS). Partial loss of AR function results in male infertility and varying degrees of incomplete masculinization. Complete loss of AR function results in an external female genital phenotype in the genetic male (8, 9). Mutations in the AR gene occur in the human population with a frequency of ~0.002%, with single base changes overwhelmingly positioned in the highly structured ligand binding domain. Mutations in the AF2 region of the ligand binding domain can cause AIS without altering equilibrium androgen binding affinity (10, 11).

For the steroid receptors as a group, AF2 serves as a critical if not essential binding site for the L*XX*LL motifs of SRC/p160 coactivators that have histone acetyltransferase activity (12). However, AR is unique because AF2 displays different affinities for multiple L*XX*LL-related motifs. Like other steroid receptors in the presence of agonist, AR AF2 binds the L*XX*LL motifs of SRC/p160 coactivators but with an affinity 5–10 times weaker than that of the AR NH_2-terminal F*XX*LF motif sequence ^{23}FQNLF^{27} (10, 13, 14). AR F*XX*LF motif binding to AF2 mediates the androgen-dependent NH_2- and carboxyl-terminal (N/C) interaction that has been shown to be important for androgen-regulated gene expression (11, 15). AR has in addition an NH_2-terminal W*XX*LF-binding motif (^{433}WHTLF^{437}) that contributes to the N/C interaction by binding AF2 (14, 16, 17). AR transactivation through AF2 in the presence of agonist appears to be limited not only by the lower binding affinity for the coactivator L*XX*LL motifs but also through competitive inhibition of coactivator binding by the AR F*XX*LF motif.

Beneath the exterior surface of the AR AF2 coactivator-binding site is a shallow interface juxtaposed against the ligand binding pocket. This close structural arrangement provides a platform for potential communication between AF2 and bound ligand in regulating AR transcriptional activity. Support for structural communication at this boundary region is evident from the slower androgen dissociation that results from F*XX*LF motif binding to AF2 (11, 15, 18). Coactivator L*XX*LL motif binding may similarly induce conformational changes in AF2 and impact ligand binding kinetics (13, 16). Here we investigated structural features and functional consequences of the naturally occurring AR germ line and somatic mutations in or near the AF2 site in search of evidence for a structural relay between AF2 and the ligand binding pocket. In the AR-linked disorders of androgen insensitivity and prostate cancer, AR gene mutations have opposite effects on AR activity that

* This work was supported by United States Public Health Service Grant HD16910 from the NICHD, by cooperative agreement U54-HD35041 as part of the Specialized Cooperative Centers Program in Reproductive Research of the National Institutes of Health, and by Fogarty International Center Grant R03TW001234 (to B. H.) Training and Research in Population and Health (to F. S. F.) by the National Institutes of Health. The costs of publication of this article were defrayed in part by the payment of page charges. This article must therefore be hereby marked "*advertisement*" in accordance with 18 U.S.C. Section 1734 solely to indicate this fact.

[1] Present address: M533 DeBakey Bldg., Dept. of Molecular and Cellular Biology, Baylor College of Medicine, One Baylor Plaza, Houston, TX 77030

[2] To whom correspondence should be addressed: Laboratories for Reproductive Biology, CB 7500, University of North Carolina, Chapel Hill NC 27599-7500. Tel.: 919-966-5168; Fax: 919-966-2203; E-mail: emw@med.unc.edu.

[3] The abbreviations used are: AR, androgen receptor; WT, wild type; GST, glutathione *S*-transferase; DHT, dihydrotestosterone; AF, activation function; AIS, androgen insensitivity syndrome; GR, glucocorticoid receptor; N/C, NH_2/carboxyl-terminal interaction; R1881, 17α-methyltrienolone.

involve the N/C interaction, androgen dissociation rates, and coactivator recruitment.

EXPERIMENTAL PROCEDURES

Plasmids—pCMVhAR vectors expressing full-length human AR with the following mutations were described: I737T and F725L (10, 19); V889M (20); E897K and I898T (10); K720A (4, 10); H874Y (21); and T877A (22). Other vectors used were as follows: VP-AR-(1–660) (11, 14); transcriptional intermediary factor 2 (TIF2)-AR fusion protein TIF2(L*XX*LL)$_3$AR-(172–919) (18); pSG5-TIF2 and VP-TIF2-(624–1287) (VP-TIF2.1) (23); wild-type and mutant pcDNA3-AR-(624–919) (10, 14); and 5XGAL4Luc3 (16). GST-SRC1-IV (GST-SRC1-(1139–1441)) was created by digesting GAL-SRC1-(1139–1441) with XbaI (blunt-ended) and BamHI, and the fragment was subcloned into pGEX-3X digested with EcoRI (blunt-ended) and BamHI. GST-AR-(4–52) (GST-AR-F*XX*LF) was created by PCR amplifying pACT2-AR-(4–52), digesting the fragment with EcoRI and XhoI, and subcloning into pGEX-4T-1 digested with the same enzymes. AIS and prostate cancer mutations were introduced into GAL-AR-(624–919) by PCR amplification of the corresponding mutant pCMVhAR and cloning the XbaI and NdeI fragments into GAL-AR-(624–919) digested with the same enzymes. pCMVhAR-(507–919) vectors (2) containing the indicated mutations were created by digesting full-length mutant pCMVhAR with KpnI and BamHI and cloning the fragment into pCMV5 digested with the same enzymes. pCMVhAR vectors containing AIS mutations G743V, Q733A, L712F, and V715M were created using a double PCR strategy. TIF2(L*XX*LL)$_3$AR-(172–919)-A*XX*AA containing the V715M or H874Y mutation was constructed by digesting the corresponding pCMVhAR mutant with HindIII and XbaI. The fragments were subcloned into similarly digested TIF2(L*XX*LL)$_3$AR-(172–919)-A*XX*AA. TIF2(L*XX*LL)$_3$AR-(172–919)-A*XX*AA-T877A was created by digesting GAL-AR-(624–919)-T877A with Csp45I and XbaI and inserting the fragment into TIF2(L*XX*LL)$_3$AR-(172–919)-A*XX*AA digested with the same enzymes. TIF2(L*XX*AA)$_3$AR-(172–919) vectors containing V715M, H874Y, and T877A were created by digesting the corresponding pCMVhAR mutant with Csp45I and XbaI and inserting the fragment into similarly digested TIF2(L*XX*AA)$_3$AR-(172–919). All PCR amplified regions were verified by DNA sequencing.

Crystal Structure Analysis—Coordinates of the wild-type AR ligand binding domain bound with R1881 and either AR-(20–30)-F*XX*LF peptide RGAFQNLFQSV, TIF2 L*XX*LL peptide KENALLRYLLDKDD, or no peptide, Protein Data Bank (www.rcsb.org) access codes 1XOW, 2AO6, and 1XQ3, respectively (13), were examined with regard to the functional data from AR mutations in AIS and prostate cancer. The structures were viewed with QUANTA (Accelrys, Inc.) and rendered and annotated with PyMol version 0.98 (Delano Scientific, www.pymol.org) and Adobe Photoshop.

Cell Transfections—Transcriptional activities of wild-type and mutant full-length human AR (pCMVhAR) were determined in transient cotransfection assays. Monkey kidney CV1 cells were maintained in Dulbecco's modified Eagle's medium containing 10% bovine calf serum, 2 mM L-glutamine, 20 mM Hepes, pH 7.2, penicillin, and streptomycin. CV1 cells (4.2×10^5/6 cm dish) were plated in the same medium except containing 5% bovine calf serum, and the next day the cells were transfected with 0.1 μg of wild-type or mutant pCMVhAR and 5 μg of the PSA-Enh-Luc reporter (Michael Carey, University of California Los Angeles) (4). For the effects of SRC/p160 coactivators, pSG5-TRAM1 (2 μg DNA/6 cm dish) was included. After incubating with the calcium phosphate-DNA precipitate for 4 h at 37 °C, cells were shocked with 15% glycerol-containing medium, washed, and transferred to serum-free medium lacking phenol red in the absence and presence of the indicated steroids. Cells were incubated overnight and the next day placed in serum-free medium with and without the indicated hormones. The medium was exchanged and incubated for an additional 24 h at 37 °C with or without hormone. Cells were washed with phosphate-buffered saline and harvested in 0.5 ml of lysis buffer containing 25 mM Tris phosphate, pH 7.8, 2 mM EDTA, 1% Triton X-100. After 30 min rocking at room temperature, 100-μl aliquots were analyzed for luciferase activity using an automated LumiStar Galaxy (BMG Labtech) multiwell plate reader luminometer.

Two-hybrid interaction assays were performed using human epithelioid cervical carcinoma HeLa cells. HeLa cells were maintained in Eagle's minimum essential medium (Invitrogen) supplemented with 10% fetal bovine serum (Sigma), 2 mM L-glutamine, penicillin, and streptomycin. HeLa cells were plated in 12-well plates (5×10^4 cells/well) and transfected using Effectene (Qiagen) or FuGENE (Roche Applied Science) with 50 ng/well GAL-AR-(624–919), 50 ng/well VP-AR-(1–660), and 0.1 μg of 5XGAL4Luc3 reporter vector. For the Effectene procedure, the DNA transfection mixture contained 50 μl of transfection buffer (Qiagen), 1 μl of Enhancer, and 1 μl of Effectene per well (4). To each DNA mixture was added 0.4 ml of serum-containing medium, and 0.4 ml was added to each well containing 0.8 ml of fresh serum-containing medium. For the FuGENE transfection, 43 μl of serum-free medium and 0.6 μl of FuGENE were combined per well, and after a 15-min incubation with the DNA, 40 μl of the mixture was added per well. After 24 h, cells were washed, and serum-free medium (2 ml) lacking phenol red was added with and without the indicated steroids. Cells were incubated overnight, and 100 μl of the cell lysate was assayed for luciferase activity after harvesting in 0.25 ml of lysis buffer as described above. Transcription assays of AR activity were performed in HeLa cells as described above using per well of 12-well plates the following: 10 ng of wild-type or mutant pCMVhAR, 0.25 μg of PSA-Enh-Luc, in the absence and presence of 50 ng/well pSG5-TIF2.

In Vitro Binding Assays—Competitive binding and ligand dissociation studies were performed at 37 °C in whole cell binding assays by plating 4×10^5 COS cells/well of 6-well plates and transfecting 1 μg of wild-type or mutant pCMVhAR or pCMVhAR-(507–919) per well using DEAE-dextran (4). Cells were incubated for 2 h at 37 °C in 0.6 ml of serum-free medium lacking phenol red and containing 5 nM [^{3}H]R1881 (17α-methyl-[^{3}H]methyltrienolone; 82 Ci/mmol), [1,2,4,5,6,7-^{3}H]dihydrotestosterone (DHT, 124 Ci/mmol), or [1,2,6,7-^{3}H]testosterone (78.5 Ci/mmol) (PerkinElmer Life Sciences). Nonspecific binding was determined by the addition of a 100-fold molar excess of unlabeled androgen. For competitive binding studies, increasing concentrations of unlabeled ligands were added during the 2-h incubation. For ligand dissociation studies, unlabeled androgen was added to the labeling media in 0.1 ml of medium to a final concentration of 50 μM, and ligand dissociation at 37 °C was terminated at increasing time intervals up to 2.5 h. Cells were washed with phosphate-buffered saline, and total bound radioactivity was determined by lysing cells in 0.5 ml of 2% SDS, 10% glycerol, and 20 mM Tris, pH 6.8. Dissociation half-times were determined as the mean ± S.E. of the time required to reduce specific androgen binding activity by 50%.

Equilibrium binding constants were determined by transfecting 2×10^5 COS cells/well of 12-well plates with 0.05 μg of wild-type and mutant pCMVhAR expression vector DNA using DEAE-dextran. Cells were incubated with 0.1, 0.2, 0.4, 0.8, 1.5, and 3 nM [^{3}H]R1881 in the absence and presence of a 100-fold molar excess of unlabeled R1881 to assess nonspecific binding. Free [^{3}H]R1881 was determined after the 2-h incubation by counting an aliquot of the medium. Cells were washed and harvested, and radioactivity was determined. In the *in vitro*

TABLE 1

[^{3}H]R1881 dissociation and affinity constants from AR AF2 mutants

Helix position in the ligand binding domain is indicated for AR AIS and charge clamp mutations. AIS grade is based on a 1–7 scale where grade 1 is mild AIS, and grades 6 and 7 are complete AIS (9). Half-times ($t_{½}$ in min) of [^{3}H]R1881 dissociation were determined at 37 °C in COS cells for full-length wild-type and mutant AR-(1–919) and AR DNA and ligand binding domain fragment AR-(507–919). Equilibrium binding affinities (K_d, nM) for full-length wild-type and mutant AR were determined by Scatchard plot analysis. Shown are the means ± S.E. determined from at least three independent assays. Nucleotide base changes are indicated for AR mutations in AIS. Diss indicates dissociation.

	Helix	AIS grade	Full-length AR		AR-(507–919), Diss $t_{½}$ min	Codon change	Ref.
			Diss $t_{½}$ min	K_d			
				nM			
AR-WT			107 ± 5	0.40 ± 0.20	33 ± 9		
F725L	3/4 loop	3–5	86 ± 5	0.82 ± 0.32	31 ± 2	TTC→CTC	10, 19
I737T	4	1–3	81 ± 3	0.44 ± 0.20	38 ± 0	ATT→ACT	10, 19
G743V	5	4–5	58 ± 6	0.16 ± 0.06	19 ± 3	GGG→GTG	76–78
Q733H	4	3–4	34 ± 3	0.30 ± 0.30	30 ± 4	CAG→CAT	79, 80
L712F	3	3	26 ± 3	0.42 ± 0.17	20 ± 1	CTT→GTT	81
I898T	12	6	21 ± 2	0.34 ± 0.02	6 ± 2	ATT→ACT	10, 80
V889M	11/12 loop	6	9 ± 1	0.46 ± 0.25	4 ± 2	GTG→ATG	82–86
K720A	3		101 ± 14	0.54 ± 0.15	27 ± 4		
E897K	12		38 ± 4	0.52 ± 0.18	34 ± 5		

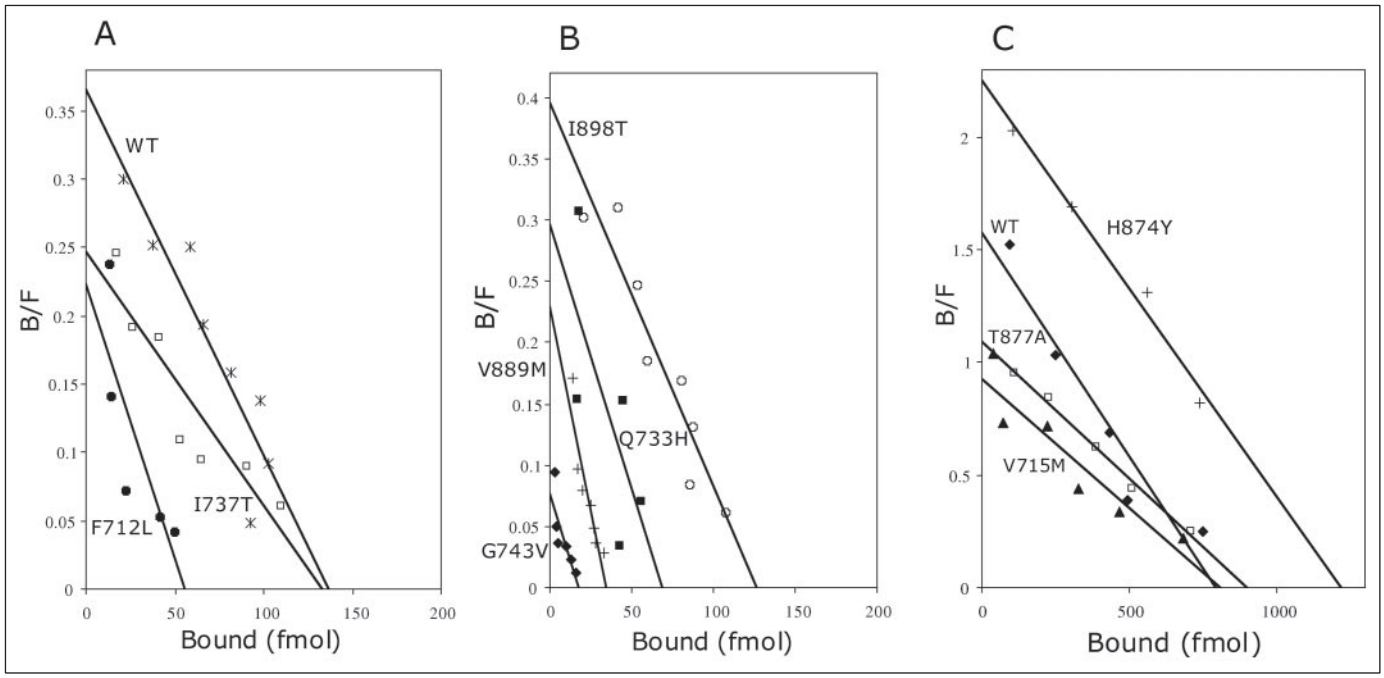

FIGURE 1. **Scatchard plots of [^{3}H]R1881 binding to wild-type AR and AR AIS and prostate cancer mutants.** Equilibrium androgen binding affinities were determined at 37 °C in cultured COS cells transiently expressing wild-type (*WT*) and mutant AR as described under "Experimental Procedures." *A* and *B*, representative data are shown for full-length WT AR and AR AIS mutants I737T, F712L, I898T, Q733H, V889M, and G743V. *C*, representative data are shown for full-length WT AR and AR prostate cancer mutants H874Y, T877A, and V715M. Apparent equilibrium androgen binding affinities (see Table 1) were determined from the means of at least three independent experiments. *B/F*, bound/free.

affinity matrix binding assays, GST fusion proteins were expressed, isolated, and incubated with [^{35}S]methionine-labeled AR ligand binding domain residues 624–919 as described (10, 14).

Degradation Assays—Wild-type and V715M, H874Y, or T877A pCMVhAR (10 μg/10-cm dish) was expressed in COS cells (2×10^6/10-cm dish) plated in Dulbecco's modified Eagle's medium containing 10% bovine calf serum (Hyclone) and transfected using DEAE-dextran. After 24 h, transfected cells were placed in serum-free medium. 48 h from transfection, cells were incubated for 20 min at 37 °C in serum-free medium lacking phenol red and methionine. To the NEG-772 Easytag Express protein labeling mixture, L-[^{35}S]methionine (1175 Ci/mmol; PerkinElmer Life Sciences) was added at 80 μCi/dish, and cells were incubated for 20 min at 37 °C. The medium was changed to serum-free without phenol red and containing 2 mM cold methionine and 1 nM testosterone, and cells were incubated for the indicated times. At each time point the medium was replaced on all plates. At the indicated times, cells were washed and harvested in phosphate-buffered saline and lysed in freshly prepared RIPA buffer (1 ml/dish) containing 1% Triton X-100, 1% deoxycholate, 0.1% SDS, 0.15 M NaCl, 5 mM EDTA, 50 mM Tris-HCl, pH 7.4, proteinase inhibitor mixture (Roche Applied Science), 1 mM dithiothreitol, and 1 mM phenylmethylsulfonyl fluoride (Sigma). Cell extracts were incubated with 25 μg of AR52 IgG antibody and 10 μl of protein A-agarose beads (Sigma) for 2 h at 4 °C. Affinity beads were centrifuged and washed with RIPA buffer, and protein was eluted in 50 μl of sample buffer containing 4% SDS, 20% glycerol, 0.2% 2-mercaptoethanol, and 20 mM Tris-HCl, pH 6.8, and separated on 10% acrylamide gels containing SDS. The gel proteins were transferred to nitrocellulose membranes and exposed to x-ray film. Degradation half-times were determined from semi-logarithmic plots of optical density of the scanned AR bands *versus* time and are expressed as the mean half-time and standard error to reduce AR levels by 50% from three independent experiments.

RESULTS

Rapid Dissociation of Bound Androgen Correlates with Reduced AR Activity in Vivo—The relationship between androgen dissociation rate and AR functional activity was investigated by characterizing naturally occurring ligand binding domain germ line mutations in AF2 and flanking regions that cause partial or complete AIS. AR mutations L712F, F725L, Q733H, I737T, G743V, V889M, and I898T result from single base changes in the coding sequence. Equilibrium binding affinities (K_d) for [^{3}H]R1881 (a synthetic androgen) were similar to that of wild-type AR (Table 1). Representative Scatchard plot analysis of the AR AIS mutants is shown in Fig. 1, *A* and *B*. On an AIS grading scale of 1–7 (9), the 46,XY genetic males had phenotypes that ranged from the mildest grade 1 with normal male external genitalia and gynecomastia (I737T), moderate grades 3–5 with ambiguous genitalia (F725L, I737T, G743V, Q733H, and L712F), and complete AIS grade 6 with external female phenotype (I898T and V889M) (9).

The dissociation half-time ($t_{½}$) of [^{3}H]R1881 for full-length wild-type AR expressed in COS cells at 37 °C was 107 min (Table 1). More rapid androgen dissociation was observed for AR with mutations F725L and I737T ($t_{½}$ = 81–86 min), G743V, Q733H, and L712F ($t_{½}$ = 26–58 min), and I898T and V889M ($t_{½}$ = 9–21 min) (Fig. 2*A*). Mean half-times of [^{3}H]R1881 dissociation (Table 1) suggest that faster androgen dissociation correlates with a more severe AIS phenotype. By comparison, AF2 charge clamp mutation K720A did not alter androgen dissociation, whereas E897K caused more rapid androgen dissociation. Neither charge clamp mutation has been reported in AIS.

Androgen dissociation rates were also measured for AR-(507–919), an AR DNA and ligand binding domain fragment that lacks the NH_2-terminal region. Androgen dissociation from AR-(507–919) ($t_{½}$ = 33 min) is ~3 times faster than from full-length AR (Table 1), reflecting the absence of the N/C interaction (14). Apparent equilibrium binding affinity of AR-(507–919) for [^{3}H]R1881 is nevertheless similar to that of wild-type full-length AR (20). Naturally occurring mutations can therefore alter androgen dissociation kinetics through different mechanisms. Mutations in AF2 can directly interfere with F*XX*LF motif binding in the N/C interaction, alter a ligand entry and exit gateway, or have indirect effects through structural changes in AF2 and the ligand binding pocket. Studies using AR-(507–919) allowed us to distinguish these possibilities.

Androgen dissociation from AR-(507–919) containing F725L, I737T, or Q733H ($t_{½}$ = 30–38 min) was similar to that of wild-type AR-(507–919) (Fig. 2*B* and Table 1), indicating this subgroup of AR mutations in AIS does not directly alter ligand entry or exit from the binding pocket. AR-(507–919) containing G743V or L712F increased androgen dissociation ($t_{½}$ = 19–20 min), and I898T and V889M caused the most rapid rates of androgen dissociation ($t_{½}$ = 4–6 min) (Fig. 2*B* and Table 1) (10).

The results suggest that F725L, I737T, and Q733H located in helices 3–5 alter ligand dissociation indirectly in the ligand binding pocket through changes at the AF2 surface that interfere with the N/C interaction. This subgroup of mutations cause partial AIS with phenotypic variation (Table 1). The rapid androgen dissociation rate of AR-(507–919) I898T suggests AF2 residue Ile-898 also impacts the ligand binding pocket from the AF2 surface. The fast androgen dissociation caused by V889M in the 11/12 loop at the base of helix 12 outside the ligand binding pocket suggests Val-889 is involved as gatekeeper for ligand entry and exit. Both I898T and V889M caused grade 6 complete AIS.

AR AF2 Mutations That Cause AIS Interfere with AR FXXLF and Coactivator LXXLL Motif Binding—A mammalian two-hybrid assay revealed that these AR AIS AF2 mutations inhibited F*XX*LF and L*XX*LL binding to a similar extent. GAL-AR-(624–919) containing the AR ligand binding domain was coexpressed with VP-AR-(1–660) containing AR NH_2-terminal F*XX*LF motif sequence ^{23}FQNLF^{27} (Fig. 3*A*) or VP-TIF2-(624–1287) containing the three L*XX*LL motif regions of TIF2 (Fig. 3*B*). Relative to the wild-type AR ligand binding domain interaction, only 5–30% luciferase activity remained for the AIS mutants in the presence of 0.1 and 1 nM DHT. Similarly, charge clamp mutation

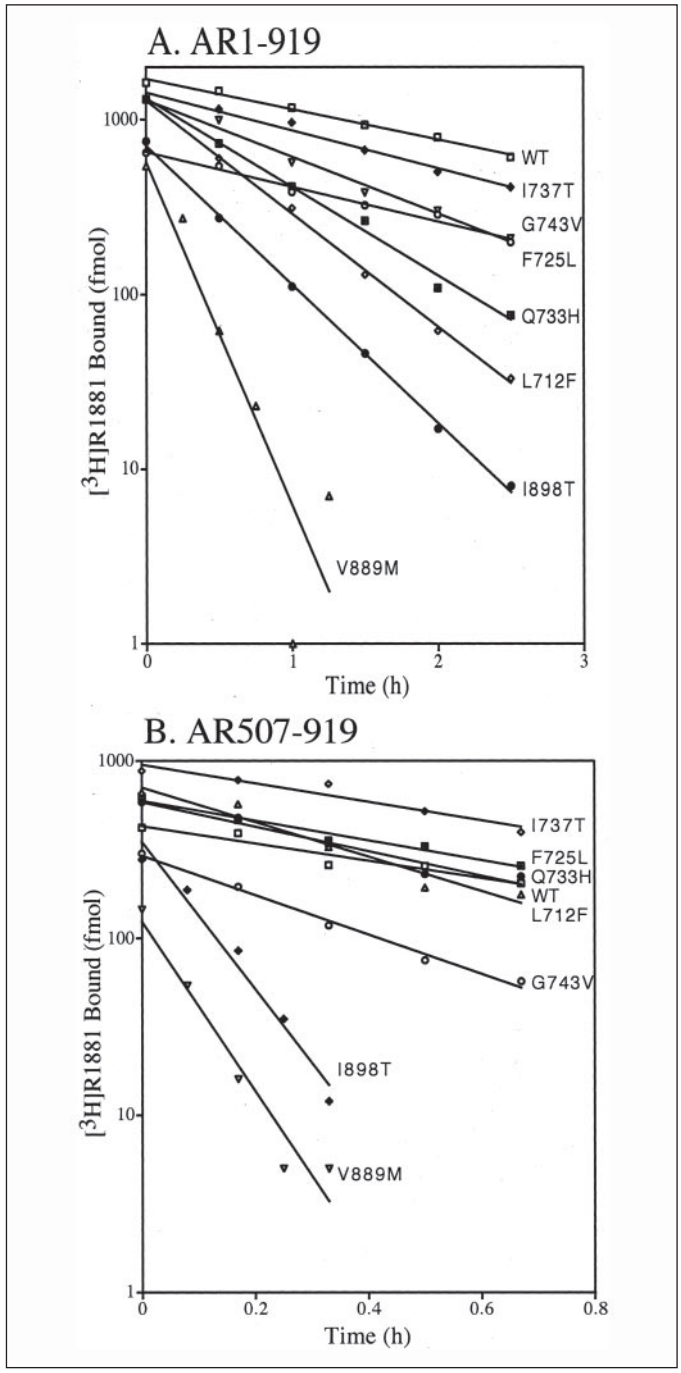

FIGURE 2. **Increased androgen dissociation of AR AIS mutations.** Dissociation rates of [^{3}H]R1881 were measured at 37 °C in cultured COS cells transiently expressing wild-type (*WT*) and mutant AR and AR-(507–919) as described under "Experimental Procedures." *A*, representative data are shown as indicated for full-length WT AR (AR-(1–919)) and AR AIS mutants I737T, G743V, F725L, Q733H, L712F, I898T, and V889M. *B*, representative data are shown as indicated for AR-(507–919), a DNA and ligand binding domain fragment, with WT sequence and AR-(507–919) mutants I737T, F725L, Q733H, L712F, G743V, I898T, and V889M. Dissociation half-times (see Table 1) were calculated from three independent experiments and are the mean times required for 50% reduction in binding activity.

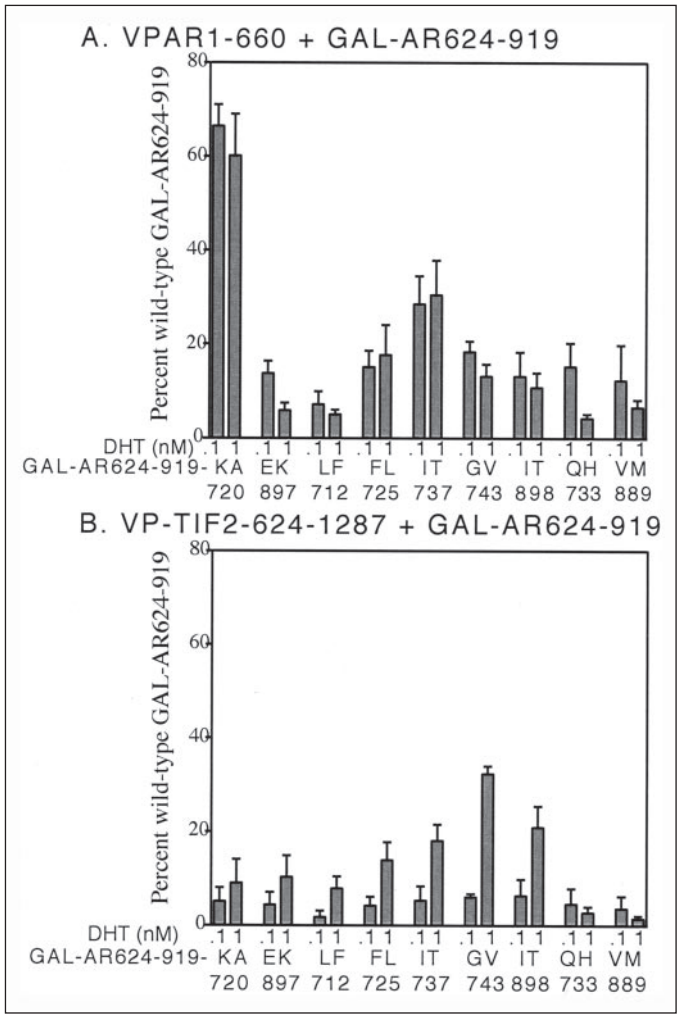

FIGURE 3. **Effect of AIS and charge clamp mutations on AR F*XX*LF and TIF2 L*XX*LL motif binding to AF2 in the AR ligand binding domain.** In two-hybrid interaction assays, HeLa cells (50,000 cells/well of 12-well plates) were transfected using Effectene or FuGENE with 0.1 μg/well 5XGAL4Luc reporter vector. *A*, VP-AR-(1–660) (50 ng/well) containing the VP16 transactivation domain and AR NH_2-terminal and DNA binding domain residues 1–660 was transfected with the indicated GAL-AR-(624–919) mutants (50 ng/well) containing the AR ligand binding domain with wild-type sequence or the indicated mutation. *B*, VP-TIF2-(624–1287) (50 ng/well) containing the VP16 transactivation domain and the TIF2-(624–1287) three L*XX*LL motif region was transfected with the indicated GAL-AR-(624–919) mutants (50 ng/well). Transfected cells were incubated for 24 h in the absence and presence of 0.1 and 1 nM DHT. Shown is the mean percent activity and error of the GAL-AR-(624–929) mutants compared with the activity of wild-type GAL-AR-(624–929) from at least four independent measurements.

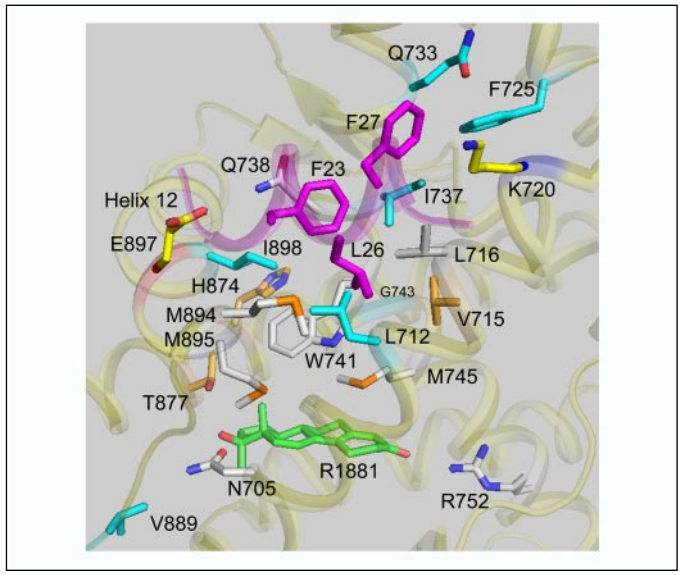

FIGURE 4. **Wild-type AF2 and ligand binding pocket region of the AR ligand binding domain bound with R1881 and AR-(20–30) F*XX*LF peptide (Protein Data Bank access code 1XOW).** Ribbon rendering is used to represent the ligand binding domain (translucent *yellow* backbone) and AR F*XX*LF peptide ^{20}RGAFQNLFQSV^{30} (translucent *magenta* backbone with opaque *magenta* side chains for Phe-23, Leu-26, and Phe-27). Wild-type AR side chains altered in AIS (*cyan*) and prostate cancer (*orange*) are illustrated along with charge clamp residues Glu-897 (translucent *red* backbone, *yellow* side chain, and *red* oxygen) and Lys-720 (translucent *blue* backbone, *yellow* side chain, and *blue* nitrogen), ligand binding pocket residues Asn-705, Trp-741, Met-745, Arg-752 (*gray* side chains, *blue* nitrogen, *red* oxygen, and *orange* sulfur), and R1881 (*green* carbon and *red* oxygen).

E897K disrupted both F*XX*LF and L*XX*LL motif binding, whereas K720A selectively inhibited L*XX*LL motif binding.

Structure Analysis and Predictions for AR Mutations in AIS—Cocrystal structures of the R1881-AR ligand binding domain complex bound to the F*XX*LF or L*XX*LL motif peptide demonstrated similar yet distinctive properties (13). The sites of 5 of the 7 residues mutated in AIS lie in close proximity to the bound F*XX*LF peptide (*magenta* in Fig. 4 and 5) or L*XX*LL peptide (not shown). Interatomic distances between wild-type residues mutated in AIS (*cyan* in Figs. 4 and 5) and the bound F*XX*LF or L*XX*LL peptide motifs are summarized in Table 2.

Our structural analysis began with mutations near the Phe-23 $i + 1$ residue of F*XX*LF that cause a spectrum of AIS phenotypes (Table 1), where $i + 1$ to $i + 5$ designate residues of the F*XX*LF and L*XX*LL motifs. AF2 residues Leu-712 (helix 3, H3), Ile-737 (H4), and Ile-898 (H12) form a close hydrophobic cluster (designated AIS group 1) proximal to $i + 1$ nearest the ligand binding pocket (Figs. 4 and 5*A*). AIS group 1 mutations weakened motif binding and caused faster androgen dissociation kinetics, both of which interfere with AR activity *in vivo* as evidenced by the AIS phenotype.

L712F in helix 3 increased androgen dissociation from full-length AR, with a half-time similar to that of AR-(507–919) with the same mutation. This suggests the principal effect of L712F is to disrupt favorable F*XX*LF motif binding to AF2, with secondary effects in the ligand binding region. Leu-712 is 4.1 Å from Phe-23 and 3.6 Å from a prominent helix 5 residue Trp-741[4] situated above and close to the B-, C-, and D-rings of R1881 (Fig. 5*A*). Leu-712 is surrounded by hydrophobic residues $i + 4$ Leu-26, Val-716 (H3), Ile-737 (H4), and Met-894 (H12). Introduction of the large phenylalanine side chain by L712F potentially disrupts F*XX*LF motif binding by directly altering favorable hydrophobic packing and contacts to Phe-23 and Leu-26, thereby weakening the protection of bound ligand afforded by the N/C interaction. L712F may also influence Met-894, a residue adjacent to helix 12 residues Met-895, Glu-897, and Ile-898, and reduce a stabilizing effect of helix 12 on the bound ligand. Unfavorable interactions between L712F and Trp-741 independent of the N/C interaction may account for the moderately faster ligand dissociation from AR-(507–919) L712F.

In contrast, I898T in helix 12 caused complete AIS and rapid androgen dissociation from full-length AR and AR-(507–919). Ile-898 is 4.4 Å from Phe-23 of the bound peptide, 5.3 Å from Trp-741, and is surrounded by Leu-712 (H3), Gln-738 (H4), Met-895 (H12), and Gln-902 (H12). I898T introduces a polar side chain near residue Gln-738, a side

[4] From our original report (13), a recent report (75), and as shown here, the absence of a C-19 methyl group in R1881 allows the Trp-741 and Met-745 side chains to adopt a conformation that differs from previously reported AR structures bound with DHT that has the C-19 methyl (34, 38). In more recent refinements not detailed here, we found our R1881 crystallographic data to be most consistent with the Trp-741 side chain conformed in roughly equal occupancy with one rotamer very similar to that shown here with R1881 and the other similar to that seen with DHT. This further supports the ligand-dependent dynamic properties of Trp-741 in the ligand binding pocket.

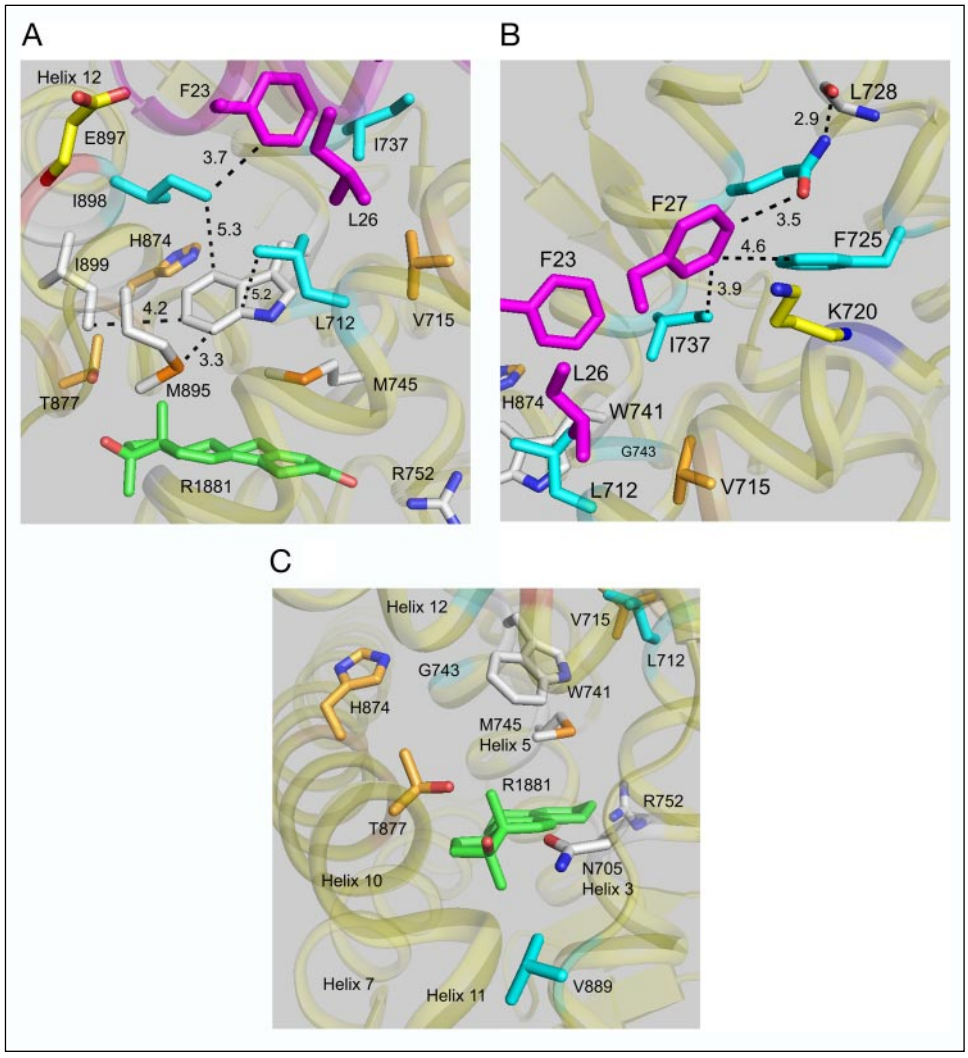

FIGURE 5. **Close up views of wild-type AR AF2 and ligand binding pocket bound with R1881 and AR-(20–30) F*XX*LF peptide (color scheme from Fig. 4).** *A,* wild-type residue side chains for group 1 AIS mutations L712F, I737T, and I898T near $i + 1$ Phe-23 of the ^{23}FQNLF^{27} motif. Leu-712 and Ile-898 are proximal to Trp-741, whereas the more distal Ile-737 lies between Phe-23 and Phe-27 as seen in *B*. Intermolecular distances (Å, *dashed black lines*) are indicated between Trp-741 to Ile-898, Leu-712, Met-895, and Ile-899. *B,* wild-type residue side chains for group 2 AIS mutations F725L, Q733H, and I737T near the $i + 5$ Phe-27 of the ^{23}FQNLF^{27} motif. Phe-725 and Gln-733 are located near the Lys-720 and the carboxyl-terminal end of the F*XX*LF motif, whereas Ile-737 is centered between Phe-23 and Phe-27. *C,* wild-type residue side chains for AIS mutants G743V and V889M. Gly-743 resides in helix 5 close to Trp-741 in the ligand binding pocket core. Val-889 in the helix 11–12 linker may serve a gatekeeper function in a possible ligand gateway near helices 3, 6, 11, and 12.

chain in wild-type AR that rearranges to stack against Phe-23 upon binding the F*XX*LF motif. I898T may contribute to a hydrogen bonding network involving side chains from Gln-738, Gln-902, and Lys-905 (H12) as evident in the peptide-free structure (13). This contribution may influence the helix 12 equilibrium to favor an unbound AF2 with reduced motif binding affinity and thus shorten the lifetime of the bound ligand. Alternatively, I898T may simply disrupt favorable hydrophobic contacts in the region by presenting too much polarity in the region near Phe-23.

In I737T, threonine again replaces isoleucine. However, I737T is less disruptive than I898T based on androgen dissociation kinetics and the AIS phenotype. Unlike Ile-898 and Leu-712, Ile-737 is centered between $i + 1$ and $i + 5$ (3.7 Å from Phe-23 and 3.9 Å from Phe-27) and more distant (6.4 Å) from Trp-741 in the ligand binding pocket compared with Leu-712 (3.6 Å) and Ile-898 (4.2 Å) (Table 2 and Fig. 5, *A* and *B*). I737T in helix 4 introduces a polar side chain into a richly hydrophobic region comprised of Leu-712, Val-715, Val-716, Ala-719, Phe-725, Val-736, Leu-812, Ile-898, and the $i + 1$ Phe-23 and $i + 5$ Phe-27 residues. The near wild-type ligand dissociation half-time for AR-(507–919) I737T but the faster dissociation half-time for full-length AR I737T compared with wild-type AR suggests that I737T interferes with F*XX*LF motif binding at the $i + 1$ and $i + 5$ sites by disrupting local hydrophobic interactions with adjacent AF2 residues rather than greatly disturbing residues in the ligand binding domain interior.

A second AF2 hydrophobic center (designated AIS group 2) is comprised of residues Phe-725 (H3′), Gln-733 (H4), and Ile-737 (H4) from AIS group 1. These residues reside within 4.6 Å of $i + 5$ of either bound peptide near the Lys-720 charge clamp (Figs. 4 and 5*B*), and Gln-733 and Phe-725 are more remote to the ligand-binding site than is Ile-737. AIS group 2 mutations account for reduced motif binding and shorter androgen dissociation half-time, both of which interfere with AR activity *in vivo* evidenced by the AIS phenotype. AR F725L and I737T modestly shortened the R1881 dissociation half-time compared with Q733H. The greater effect of Q733H may arise from a change in the 3 Å hydrogen bond contributed by Gln-733 N-ϵ2 to the Leu-728 backbone carbonyl, as well as the introduction of the polar aromatic imidazole side chain near $i + 5$ Phe-27 and Phe-725 (Fig. 5*B*). F725L preserves the hydrophobic character of the region, even though a large planar phenyl ring is replaced by the smaller branched leucine side chain that would alter the shape complementarity and regional hydrophobic contacts between Phe-725 and the $i + 5$ site. Given their close proximity to $i + 5$ and remote location to the ligand binding pocket and near wild-type ligand dissociation rate of AR-(507–919), AIS mutations F725L and Q733H most likely decrease androgen retention times by directly interfering with F*XX*LF motif binding in the $i + 5$ region.

The remaining two AIS mutations, G743V and V889M, respectively, cause moderately severe and complete AIS in correlation with the ligand dissociation kinetics in Table 1. Gly-743 in helix 5 located just

outside AF2 in the hydrophobic core near Trp-741, Met-745, and the ligand binding pocket (Fig. 5*C*) faces Val-866 in helix 10 and is surrounded by Met-742 (H5), Val-746 (H5), Leu-811 (H8), Val-866 (H10), Gln-867 (H10), and Ala-870 (H10). The 2-fold more rapid androgen dissociation half-time caused by G743V in full-length AR suggests destabilization of the ligand binding pocket and interference with ligand-dependent F*XX*LF motif binding. Replacing a flexible glycine with valine may render helix 5 too rigid to allow neighboring core residues to adjust and contact the ligand optimally or it may simply destabilize the helix 5 coil and/or key packing interactions near helices 10 and 11.

Ligand trafficking through an opening assembled by the NH_2 terminus of helix 3, helix 11, the 11–12 linker, and AF2 helix 12 was supported by the effects of V889M, a mutation that caused complete AIS. Val-889 lies in the linker region preceding the AF2 helix 12 distant from AF2 and the bound peptide motif (Fig. 4 and Fig. 5*C* and Table 2). Val-889 is near the ligand binding pocket, ~6 Å from D-ring substituents of the bound ligand and 3.5 Å from Asn-705, a residue that hydrogen bonds with the ligand C-17 hydroxyl group and is adjacent to Phe-876 (H10), Phe-891, Leu-880 (H11), Leu-701 (H3), and Phe-697 (H3). Methionine residues are notable for their flexible and accommodating side chain. However, in this case it appears that the longer side chain and large sulfur atom of V889M disturbs the largely hydrophobic region and destabilizes the linker region and equilibrium position of the AF2 helix 12. A key interaction between Asn-705 and the steroid D-ring may also be disrupted and reduce the lifetime of the bound ligand without significantly altering the equilibrium binding constant.

TABLE 2

Interatomic distances (in Å) between bound AR FXXLF peptide, TIF2 LXXLL peptide, and AR Trp-741 to AR ligand binding domain residues

Interatomic distances (Å) are from the AR F*XX*LF peptide, the TIF2 third L*XX*LL peptide, or AR Trp-741 to the indicated ligand binding domain atoms. The first residue of the F*XX*LF or L*XX*LL motif is $i + 1$. Atom designations adhere to standard IUPAC nomenclature.

AR ^{23}FXXLF^{27}		i+1			i+4			i+5			AR ^{741}W		
	AR LBD atom	F23	Å	LBD	L26	Å	LBD	F27	Å	LBD	W741	Å	LBD
Androgen Insensitivity Syndrome	F725	CZ	8.0	CZ	CD2	11.9	CE2	CE1	4.6	CE2	CG	12.7	CE1
	Q733	CE1	7.7	CB	CG	12.4	CB	CZ	3.5	OE1	CG	16.4	CD
	I737	CZ	3.7	CG2	CD2	7.5	CG2	CE1	3.9	CD1	CG	6.4	CG2
	L712	CE2	4.1	CE1	CD2	4.6	CG	CD1	8.8	CD1	CD1	3.6	CD1
	I898	CD1	3.7	CD1	CD2	7.2	CD1	CB	9.3	CD1	CE3	4.2	CG2
	V889	CD2	19.0	CG1	CD2	19.4	CG1	CB	24.2	CG1	CH2	11.6	CG1
	G743	CE2	13.7	CA	CD2	16.4	CA	CD1	17.1	CA	CD1	8.0	CA
Charge clamp	K720	CZ	7.7	CD	CG	7.9	CD	CE1	3.8	CD	CG	15.3	CE
								O	2.7	NZ			
	E897	CB	4.6	CD	CB	9.0	CD	CB	10.7	CD	CZ3	11.0	CD
		N	3.2	OE2									
Prostate Cancer	V715	CE2	7.8	CB	CD2	8.0	CB	CG	10.7	CB	CD1	5.2	CG2
	H874	CE2	12.3	NE2	CD2	15.8	NE2	CD1	16.7	NE	CE3	5.5	CD2
	T877	CD2	14.6	CG2	CD2	15.8	NE2	CD1	16.7	NE2	CZ3	5.3	CG2

TIF2 ^{740}LXXLL^{744}		i+1			i+4			i+5			AR ^{741}W		
	AR LBD atom	L745	Å	LBD	L748	Å	LBD	L749	Å	LBD	W741	Å	LBD
Androgen Insensitivity Syndrome	F725	CD2	9.3	CZ	CB	10.6	CE2	CD1	4.3	CE2	CG	12.3	CZ
	Q733	CD2	8.5	CB	CB	11.0	CB	CD2	3.7	OE1	CG	15.7	CD
	I737	CD1	4.8	CG2	CB	8.0	CD1	CD1	4.0	CD1	CG	6.2	CG2
	L712	CD1	4.5	CD1	CD1	6.1	CG	CD1	9.5	CD1	CD1	3.9	CD1
	I898	CD2	4.7	CD1	CD1	9.0	CD1	CD2	11.2	CD1	CZ3	4.1	CG2
	V889	CD1	19.6	CG1	CD1	19.9	CG1	CB	25.6	CG1	CH2	11.7	CG1
	G743	CD2	14.9	CA	CD1	17.9	CA	CD1 1	17.4	CA	CG	7.4	CA
Charge clamp	K720	CD1	8.8	CD	CB	6.4	CD	CD1	3.9	CD	CG	15.6	CE
					O	3.0	NZ	O	2.9	NZ			
	E897	CB	7.4	CD	CD1	12.0	CD	CB	14.0	CD	CZ3	11.4	CD
Prostate Cancer	V715	CD1	7.9	CB	CD1	9.0	CB	CD1	9.4	CB	CD1	4.8	CG2
	H874	CD2	12.7	NE2	CD1	12.3	NE2	CD1	17.7	NE2	CE3	5.9	CD2
	T877	CD2	12.7	CG2	CD1	17.2	OG1	CD1	20.8	CG2	CZ3	5.9	CG2

AR Mutations in Prostate Cancer Slow Androgen Dissociation—Several somatic mutations in prostate cancer occur in the AR AF2 and ligand binding region (24). These include V715M (25), H874Y (21, 26), T877A (22, 27), V730M (25, 28), and R726L (29). These prostate cancer mutations result from single base changes and do not significantly alter the apparent equilibrium binding affinity of [^{3}H]R1881 (Fig. 1*C* and Table 3). Valines 715 and 730 are in the hydrophobic core of AF2; Arg-726 is in the positive charge cluster flanking AF2 (4), and His-874 and Thr-877 are in helix 10 adjacent to AF2 helix 12. Neither V730M nor R726L change the androgen dissociation rate, and no difference from wild-type AR was observed for AR R726L in two-hybrid assays of motif binding (data not shown). R726L was identified as a germ line mutation in the Finnish population (29, 30) and lacks a strict clinical correlation with prostate cancer. V730M selectively increases SRC1 L*XX*LL motif binding (13).

Remarkably, three AR mutations in prostate cancer, V715M, H874Y, and T877A, slowed the dissociation rate of bound androgen relative to wild-type AR (Fig. 6*A*). The half-times of [^{3}H]R1881 dissociation increased 2-fold from $t_{½}$ = 107 min for wild-type AR to $t_{½}$ = 207–212 min for AR V715M, H874Y, and T877A (Table 3). Longer dissociation half-times of [^{3}H]DHT and [^{3}H]testosterone were also observed. Testosterone dissociation from AR H874Y was 4.5-fold slower than from wild-type AR. Normally testosterone dissociates ~3 times faster than DHT from full-length wild-type AR (Table 3) and is a weaker androgen *in vivo* (31).

The effects of the mutations were also evident in the absence of the N/C interaction because they slowed the dissociation of R1881 from AR-(507–919) (Fig. 6*B*). Dissociation half-times of [^{3}H]R1881 from AR-(507–919) containing V715M, H874Y, or T877A were ~2-fold longer ($t_{½}$ = 60–82 min) compared with the wild-type fragment ($t_{½}$ = 31 min) (Table 3). Other AR ligand binding domain mutations reported in prostate cancer retained high affinity equilibrium binding (8) but did not slow dissociation of [^{3}H]R1881. These included G750S ($t_{½}$ = 123 min), S782N ($t_{½}$ = 93 min), A896T ($t_{½}$ = 88 min), and L701H ($t_{½}$ = 28 min). Thus a slower androgen dissociation depends largely on the position of the mutation in the ligand binding domain.

TABLE 3

[^{3}H]Androgen dissociation and affinity constants for AR prostate cancer mutants

Helix position in the ligand binding domain is indicated for the sites of AR prostate cancer mutations. Half-times ($t_{½}$ in min) of [^{3}H]R1881, [^{3}H]DHT, and [^{3}H]testosterone (T) dissociation (Diss) were determined at 37 °C in COS cells for wild-type and mutant full-length AR (amino acid residues 1–919). [^{3}H]R1881 dissociation was determined for wild-type and mutant AR-(507–919). Equilibrium binding affinities (K_d, nM) of [^{3}H]R1881 for wild-type and mutant full-length AR were determined by Scatchard plot analysis. Binding constants are the mean ± S.E. from three independent assays. Nucleotide base changes are indicated for AR mutations in prostate cancer.

AR	Helix	Full-length AR				AR-(507–919), Diss $t_{½}$ min, R1881	Codon change
		Diss $t_{½}$ min			K_d, R1881		
		R1881	DHT	T			
					nM		
Wild-type		107 ± 5	206 ± 30	59 ± 3	0.40 ± 0.20	31 ± 3	
V715M	3	207 ± 43	298 ± 78	101 ± 5	0.79 ± 0.25	70 ± 8	GTG→ATG
H874Y	10	212 ± 53	324 ± 60	266 ± 15	0.56 ± 0.37	60 ± 7	CAT→TAT
T877A	10	208 ± 37	240 ± 48	143 ± 15	0.75 ± 0.30	82 ± 12	ACT→GCT

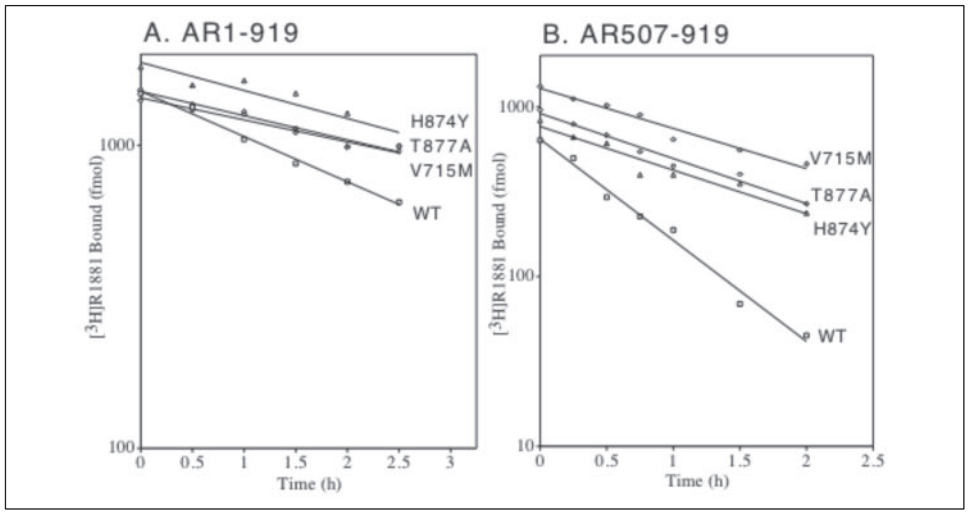

FIGURE 6. **Slower androgen dissociation of three AR prostate cancer mutants.** Dissociation rates of [^{3}H]R1881 were measured at 37 °C in cultured COS cells transiently expressing wild-type (*WT*) and mutant AR and AR-(507–919) as described under "Experimental Procedures." *A,* representative data are shown as indicated for full-length WT AR (AR-(1–919)) and AR AIS mutants H874Y, T877A, and V715M. *B,* representative data are shown as indicated for AR-(507–919) with WT sequence and AR-(507–919) mutants V715M, T877A, and H874Y. Dissociation half-times (see Table 3) were calculated from at least three independent experiments and are the mean times required for 50% reduction in binding activity.

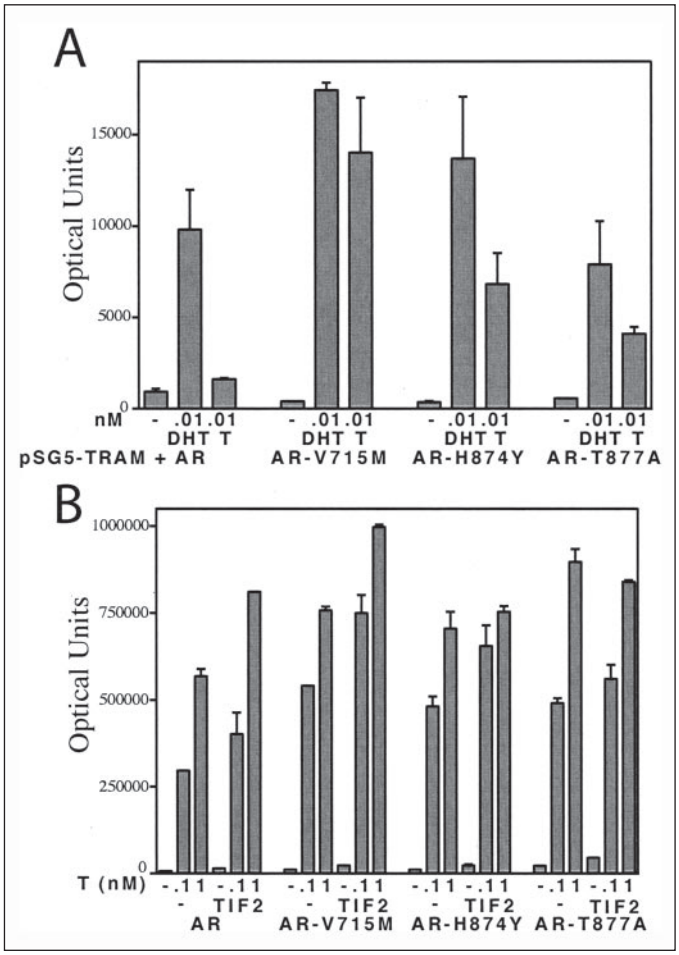

FIGURE 7. **Increased AR transactivation of AR prostate cancer mutants V715M, H874Y, and T877A.** *A,* CV1 cells (4.2×10^5/6-cm dish) were transfected using calcium phosphate DNA precipitation and per dish, 100 ng of pCMVhAR with wild-type or V715M, H874Y, or T877A mutant sequence, 2 μg of pSG5-TRAM1, and 5 μg of PSA-Enh-Luc. Transfected cells were incubated for 40 h in the absence and presence of 0.01 nM DHT or testosterone (*T*). *B,* HeLa cells (5×10^4/well of 12-well plates) were transfected using FuGENE by adding per well, 10 ng of pCMVhAR with wild-type or V715M, H874Y, or T877A mutant sequence, 0.25 μg of PSA-Enh-Luc, in the absence or presence of 50 ng of pSG5-TIF2. Transfected cells were incubated in the absence and presence of 0.1 and 1 nM testosterone (*T*), and luciferase activity was determined. Luciferase activities are representative of three independent experiments.

Increased AR Transcriptional Activity and Coactivator Recruitment—The effects of the prostate cancer mutations on AR transcriptional activity were determined in the absence and presence of SRC/p160 coactivator coexpression. With transient coexpression of p160 coactivator TRAM-1 in CV1 cells, AR V715M, H874Y, and T877A increased transcriptional activity relative to wild-type AR in response to 0.01 nM testosterone (Fig. 7*A*). Transcriptional activity was also greater with the more potent androgen DHT; however, the effects of the mutations were less evident in the presence of DHT. In the absence of transient coactivator expression or at higher levels of androgen, no major differences in AR transcriptional activity were observed in CV1 cells (data not shown). However, in HeLa cells that express higher endogenous levels of SRC/p160 coactivators (32), prostate cancer mutations V715M, H874Y, and T877A increased AR activity in the presence of testosterone (Fig. 7*B*). For AR V715M, transcriptional activity also increased with coexpression of TIF2. Increases in transcriptional activities of the three mutants over wild-type AR were noted in both cell lines in the presence of 1 nM 4-androstene-3,17-dione (data not shown).

The increase in AR transcriptional activity and slower dissociation of bound androgen by two of the mutants was associated with increased binding of the F*XX*LF or L*XX*LL motifs to the AR carboxyl-terminal region in GAL-AR-(624–919). In two-hybrid assays, V715M and H874Y increased F*XX*LF (Fig. 8*A*) and L*XX*LL (Fig. 9*A*) motif binding over that of the wild-type AR in the presence of DHT or testosterone. For the F*XX*LF motif in VP-AR-(1–660), greater increases in binding indicative of the AR N/C interaction were observed using 0.1 nM testosterone or DHT. For the L*XX*LL motif in VP-TIF2-(624–1287), increases in transcriptional activity were apparent in response to low levels of androgen. Increased F*XX*LF and L*XX*LL motif binding by the mutants relative to wild-type AR was also observed in response to the adrenal androgens, 4-androstene-3,17-dione and 5α-androstane-3α,17β-diol (Figs. 8*B* and 9*B*). However, no increase in motif binding was detected with AR T877A in the presence of these androgens (Figs. 8 and 9).

Competitive ligand binding assays confirmed that V715M, H874Y, and T877A did not alter AR binding affinity for R1881, DHT, testosterone, 4-androstene-3,17-dione, or 5α-androstane-3α,17β-diol (Fig. 10). However, as reported previously (21, 27), LNCaP cell line mutant AR T877A increased binding of hydroxyflutamide, estradiol, and progesterone (data not shown).

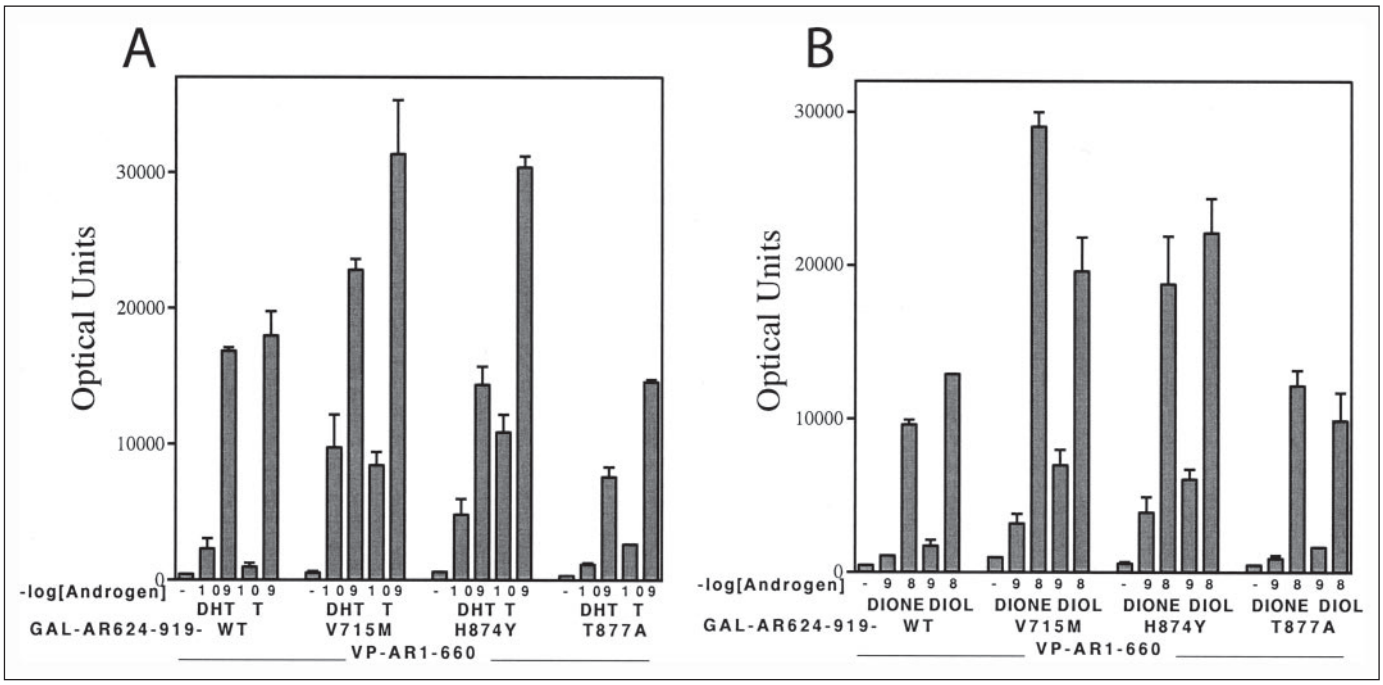

FIGURE 8. **Increase in AR F*XX*LF motif binding by prostate cancer mutations V715M and H874Y.** HeLa cells (5×10^5/well of 12-well plates) were transfected using FuGENE by adding per well, 0.1 μg of 5XGAL4Luc3, 50 ng of GAL-AR-(624–929) containing wild-type or V715M, H874Y, and T877A mutant AR ligand binding domain, and 50 ng of VP-AR-(1–660). Transfected cells were incubated for 24 h in the absence and presence of 0.1 and 1 nM DHT or testosterone (*T*) (*A*), and with 1 and 10 nM 4-androstene-3,17-dione (*DIONE*) or 5α-androstane-3α,17β-diol (*DIOL*) (*B*). Luciferase activity and error are representative of three independent experiments.

AR transcriptional activity can therefore increase as a result of AR mutations in prostate cancer through mechanisms that include increased F*XX*LF and L*XX*LL motif binding and slower dissociation rates of bound androgen. The absence of a prominent increase in F*XX*LF or L*XX*LL motif binding by T877A suggests it was the structural effects imposed by V715M and H874Y rather than the slow androgen dissociation rate *per se* that stabilized motif binding.

TIF2 LXXLL-AR Chimeras—Previously, we showed that the AR N/C interaction between the AR NH_2-terminal F*XX*LF motif and AF2 slows the dissociation of bound androgen. However, slower androgen dissociation does not occur in the presence of the L*XX*LL motif when AR was coexpressed with TIF2 (14) or in L*XX*LL-AR chimeras (18). Because the V715M and H874Y mutations increased AR F*XX*LF and TIF2 L*XX*LL motif binding to the AR carboxyl-terminal fragment, we determined whether L*XX*LL motif binding influences androgen dissociation of these mutants. Dissociation half-times of [^{3}H]R1881 were determined for TIF2-AR chimeras in which the AR NH_2-terminal region (residues 1–171) containing the F*XX*LF motif was replaced by the L*XX*LL motif region of TIF2 (residues 627–780), and the V715M, H874Y, or T877A mutation was introduced into the ligand binding domain (Table 4). For some of the chimeras, L*XX*AA replaced the TIF2 L*XX*LL motifs to establish L*XX*LL motif dependence. In others, A*XX*AA replaced the AR W*XX*LF motif at residues 433–437, a motif that contributes only weakly to the dissociation rate of bound androgen (18).

TIF2-AR chimeras with L*XX*LL or L*XX*AA TIF2 sequence had faster dissociation half-times ($t_{1/2}$ = 40–48 min) compared with full-length AR ($t_{1/2}$ = 107 min) (Table 4). This reflects the absence of the AR N/C interaction and a weaker interaction of L*XX*LL motifs to AR AF2. Introducing each of the prostate cancer mutations, V715M, H874Y, and T877A, slowed androgen dissociation, but this was independent of L*XX*LL motif binding. A notable exception was V715M, which increased binding of L*XX*AA, suggesting this mutation alters motif binding specificity.

Slow dissociation of androgen from the AR prostate cancer mutants therefore appears to result from inherent changes in the ligand binding domain rather than from increased coactivator L*XX*LL motif binding. The mutations influence the AF2 boundary with the ligand binding pocket to stabilize ligand and for two of the mutants, L*XX*LL motif binding.

Increased Motif Binding in Vitro—GST affinity matrix binding assays were used to examine further the effect of the AR prostate cancer mutations on L*XX*LL and F*XX*LF motif binding. In this assay, the fourth L*XX*LL motif of SRC1 was selected because of its relatively strong binding to the AR ligand binding domain compared with other L*XX*LL motifs (33). ^{35}S-Labeled AR ligand binding domain fragments AR-(624–919) with wild-type or V715M, H874Y, and T877A mutant sequences were incubated with GST-SRC1-IV (SRC1 residues 1139–1441) or GST-AR-F*XX*LF (AR residues 4–52) (Fig. 11). In the presence of DHT or testosterone, prostate cancer mutants AR V715M and H874Y bound the L*XX*LL and F*XX*LF motifs to a greater extent than AR T877A or wild-type AR. The data support the increase in intracellular L*XX*LL motif binding shown in Figs. 7–9 and provide further evidence that prostate cancer mutants V715M and H874Y increase L*XX*LL and F*XX*LF motif binding.

Structure Analysis and Predictions for AR Mutations in Prostate Cancer—Structure of the AR ligand binding domain complexed with R1881 and F*XX*LF or L*XX*LL peptide was analyzed in light of the AR prostate cancer mutations. The Val-715 side chain in AF2 helix 3 faces toward the ligand binding pocket and at its closest distance is ~5.2 Å from Trp-741,[4] a hydrophobic residue in helix 5 that lies directly above and contacts the bound ligand (Fig. 12). A hydrophobic space surrounding Val-715 created by residues Leu-712, Trp-718, Ile-737, Trp-741, Leu-744, and Met-745 appears to readily accommodate the V715M mutation. Compared with valine, the longer, flexible methionine side chain may better fill the space and stabilize interactions with Trp-741, possibly strengthening interactions with the ligand that are further

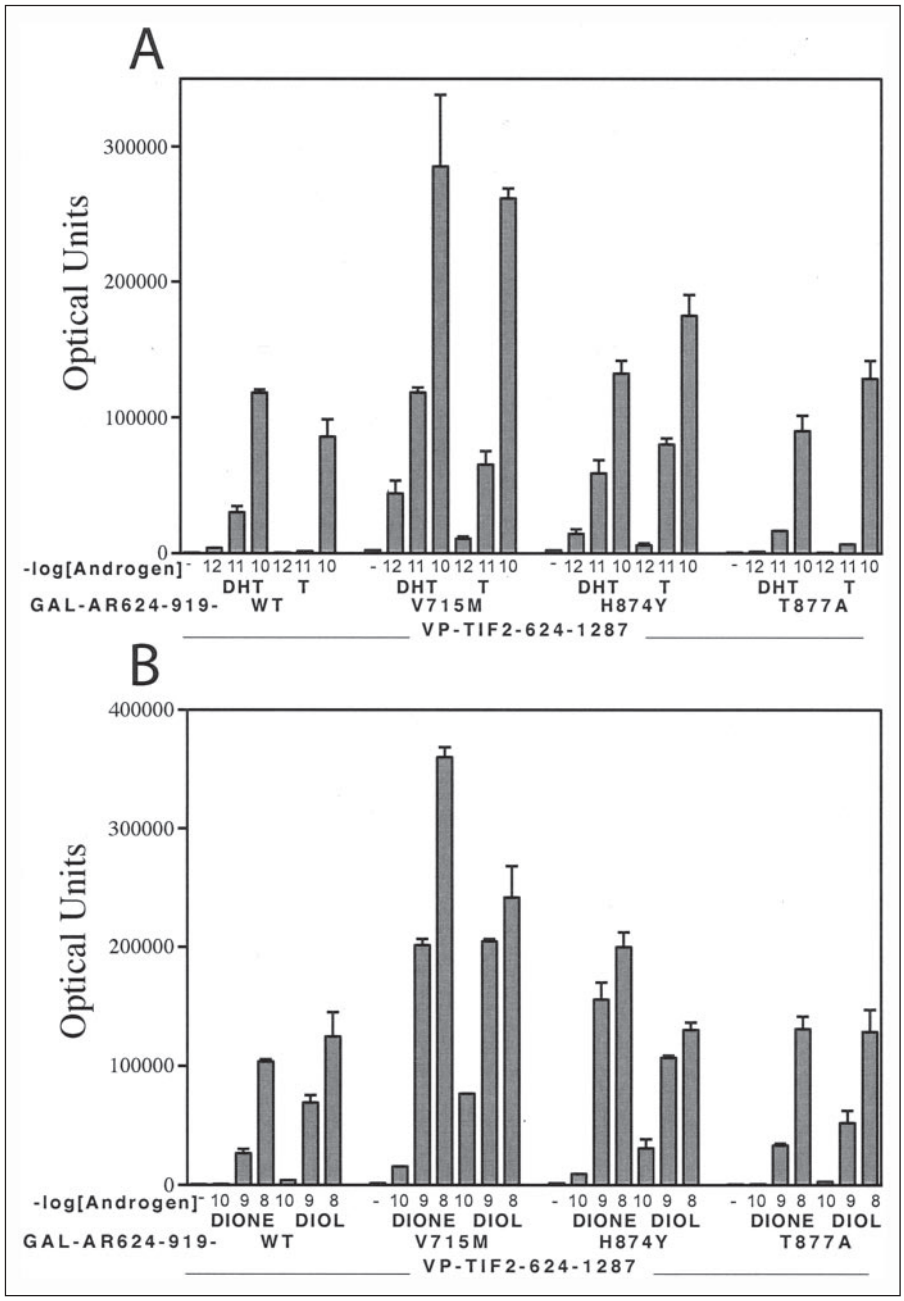

FIGURE 9. **Increase in TIF2 L*XX*LL motif binding by prostate cancer mutations V715M and H874Y.** HeLa cells (5×10^5/well of 12-well plates) were transfected using FuGENE by adding per well, 0.1 μg of 5XGAL4Luc3, 50 ng of GAL-AR-(624–929) containing wild-type or V715M, H874Y, and T877A mutant AR ligand binding domain, and 50 ng of VP-TIF2-(624–1287). Transfected cells were incubated for 24 h in the absence and presence of 0.001, 0.01, and 0.1 nM DHT or testosterone (*T*) (*A*), or 0.1, 1, and 10 nM 4-androstene-3,17-dione (*DIONE*) or 5α-androstane-3α,17β-diol (*DIOL*) (*B*). Luciferase activity and error are representative of three independent experiments.

transmitted toward the AF2 floor through Ile-898. Altered structural changes between Trp-741 and AF2 floor residues may enhance shape complementarity at the AF2 floor and facilitate F*XX*LF and L*XX*LL motif binding.

Located in helix 10, His-874 is on the opposite side of Trp-741 from Val-715 and farther from the bound peptides (Table 2) but about equidistant (5.5 Å) to Trp-741. Through a conserved water, His-874 engages in a solvent-mediated hydrogen bond to the backbone of Trp-741 in helix 5. The H874Y mutation provides more hydrophobicity with a longer hydroxylated phenyl ring that may displace the conserved water and directly hydrogen-bond to a helix 5 backbone atom. Direct hydrogen bonding could stabilize helix 5, strengthen interactions between Trp-741 and the bound ligand, and transmit stabilizing effects to the AF2 floor that enhance F*XX*LF and L*XX*LL motif binding.

Helix 10 residues Thr-877 and His-874 are similar distances from the AF2-bound peptide (Table 2) and like Val-715 are ~5.0 Å from Trp-741. However, in contrast to Val-715 and His-874, Thr-877 has direct contact with the D-ring hydroxyl of bound DHT (34) and R1881 (13) through a 2.9 Å hydrogen bond. In contrast, the slower androgen dissociation rates caused by T877A are associated with a hydrophilic to hydrophobic residue change, loss of a hydrogen bond to the ligand, and no substantial increase in F*XX*LF or L*XX*LL motif binding. It therefore appears that T877A has a different conformational effect on AF2 than that caused by the V715M and H874Y mutations.

The data indicate that all three AR prostate cancer mutations that slow the dissociation rate of bound androgen are positioned near (V715M and H874Y) or in (T877A) the ligand binding pocket and may influence the conformation of Trp-741, a hydrophobic residue that directly contacts the bound ligand. The data suggest that V715M and H874Y impact not only the ligand binding pocket to slow androgen dissociation but also the AF2 binding surface to facilitate L*XX*LL and F*XX*LF motif binding.

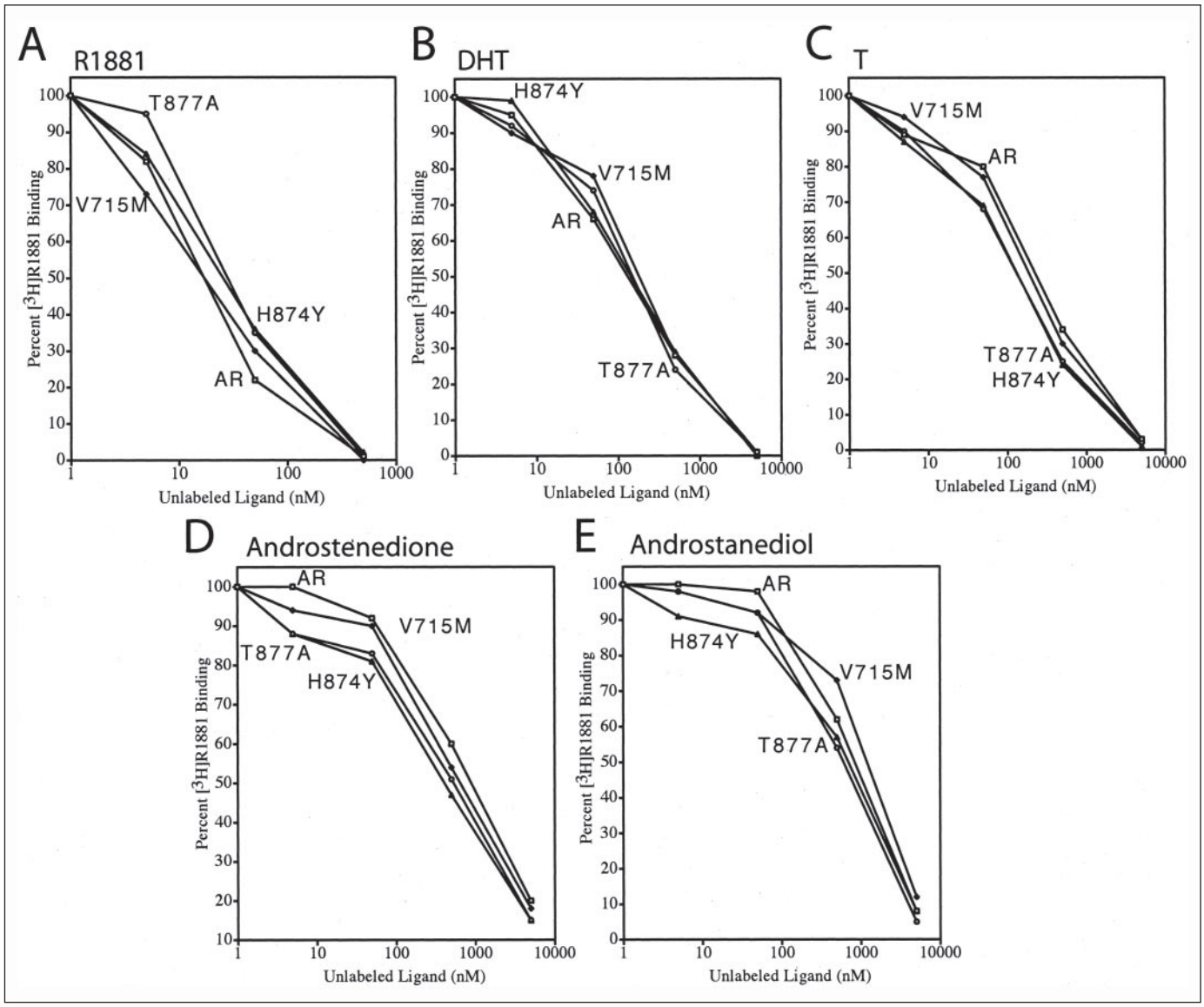

FIGURE 10. **Steroid binding specificity of AR V715M, H874Y, and T877A mutants in prostate cancer.** Competitive binding studies were performed in COS cells (4×10^5/well of 6 well plates) using the DEAE-dextran transfection method as described under "Experimental Procedures" with 2 μg/well pCMVhAR containing wild-type or V715M, H874Y, and T877A mutant sequences. Cells were incubated with 5 nM [^{3}H]R1881 in the absence and presence of increasing concentrations of unlabeled R1881 (*A*), DHT (*B*), testosterone (*T*) (*C*), 4-androstene-3,17-dione (*D*), and 5α-androstane-3α,17β-diol (*E*). Shown are the average percent competitive binding determinations from three independent experiments.

TABLE 4

[^{3}H]R1881 Dissociation of TIF2-AR prostate cancer mutation chimeras

Half-times ($t_{1/2}$ in min) of [^{3}H]R1881 dissociation (Diss) were determined at 37 °C in COS cells for AR and TIF2-AR chimeras containing TIF2-(627–780) L*XX*LL motif region expressed NH_2-terminal in fusion proteins with AR-(172–919), with and without the V715M, H874Y, or T877A mutation. L*XX*AA replaced the three TIF2 L*XX*LL motifs, and AQNAA replaced the WQNLF residues 433–437 AR region. The data are the mean ± S.E. from three independent assays.

	Diss $t_{1/2}$ min
AR	107 ± 5
TIF2(L*XX*LL)$_3$AR-(172–919)-A*XX*AA	48 ± 6
TIF2(L*XX*AA)$_3$AR-(172–919)	40 ± 5
TIF2(L*XX*LL)$_3$AR-(172–919)-A*XX*AA-V715M	77 ± 5
TIF2(L*XX*AA)$_3$AR-(172–919)-V715M	135 ± 24
TIF2(L*XX*LL)$_3$AR-(172–919)-A*XX*AA-H874Y	134 ± 6
TIF2(L*XX*AA)$_3$AR-(172–919)-H874Y	137 ± 18
TIF2(L*XX*LL)$_3$AR-(172–919)-A*XX*AA-T877A	126 ± 16
TIF2(L*XX*AA)$_3$AR-(172–919)-T877A	119 ± 21

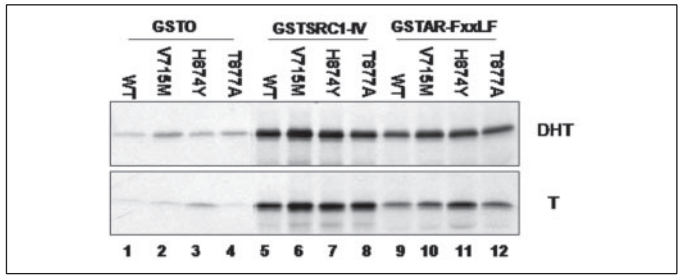

FIGURE 11. **Increased binding of L*XX*LL and F*XX*LF motifs to AR prostate cancer mutants V715M, H874Y, and T877A *in vitro*.** GST affinity matrix binding assays were performed using GST-0 empty parent vector (*lanes 1–4*), GST-SRC1-IV containing the fourth carboxyl-terminal L*XX*LL of SRC1 residues 1139–1441 (*lanes 5–8*), and GST-AR-(4–52) (GST-AR-F*XX*LF) containing the AR F*XX*LF motif in residues 4–52 (*lanes 9–12*). GST-purified extracts were incubated with pcDNA3-HA-AR-(624–919) with wild-type or V715M, H874Y, and T877A mutant sequence in the presence of 1 μM DHT or testosterone (*T*). The bands represent ^{35}S-labeled HA-AR-(624–919) with wild-type or indicated mutant sequence.

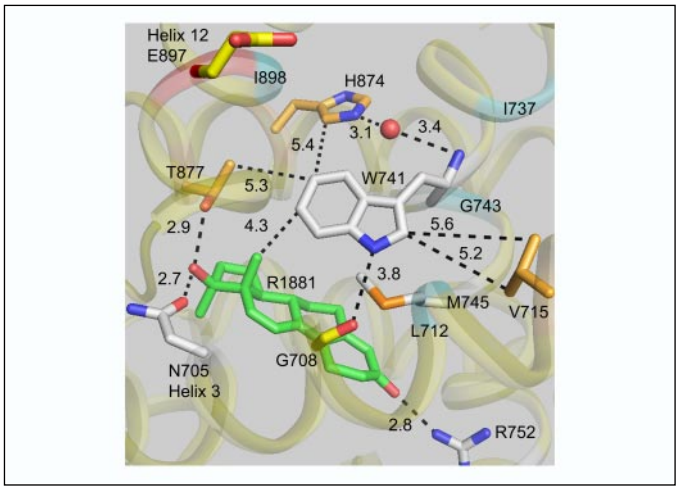

FIGURE 12. **Close up view of the wild-type AR ligand binding pocket region (color scheme from Fig. 4).** Three prostate cancer mutations, V715M, H874Y, and T877A, surround helix 5 residue Trp-741, which lies above R1881 in the steroid-binding site. The V715M mutation contributes a seventh methionine to the predominantly hydrophobic ligand binding pocket. The His-874 side chain engages in a water (*red sphere*)-mediated hydrogen bond to the backbone of Tyr-741. Residue Thr-877 and Asn-705 hydrogen-bond to the C-17 hydroxyl group on the steroid D-ring. Intermolecular distances (Å, *dashed black lines*) are indicated. The backbone of nearby AIS mutations are in *cyan*.

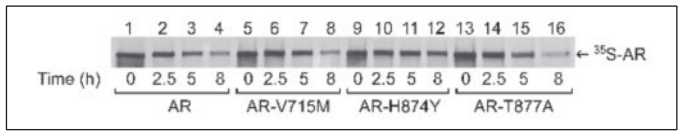

FIGURE 13. **Increased stabilization of AR prostate cancer mutants in the presence of 1 nM testosterone.** Wild-type AR or AR V715M, H874Y, and T877A in pCMVhAR (10 μg/dish) were expressed in COS cells (1.8×10^6 cells/10-cm dish) using the DEAE-dextran transfection method. Cells were placed in serum-free medium without phenol red-free 24 h after transfection, and 24 h after incubation, cells were incubated with 80 μCi of [^{35}S]methionine per plate for 20 min in the presence of 1 nM testosterone. Cells were transferred to serum-free medium containing 2 mM cold methionine and 1 nM testosterone and incubated at 37 °C for 0, 2.5, 5, or 8 h as indicated. Cells were harvested, and AR was immunoprecipitated. Mean AR degradation half-times were determined as described under "Experimental Procedures." The x-ray film was exposed for 3 days and is representative of three independent experiments.

Increased AR Stability—The F*XX*LF motif-mediated AR N/C interaction slows the dissociation rate of bound androgen and stabilizes AR (11, 18, 35). This link between androgen dissociation rate and AR stability is evident with potent androgens such as DHT (20) compared with weaker androgens such as testosterone. AR nevertheless binds testosterone with an equilibrium affinity similar to DHT, but testosterone dissociates more rapidly and is a less effective androgen *in vivo* (20, 31). We therefore investigated whether slower dissociation of testosterone from the AR prostate cancer mutants increased AR stabilization.

AR degradation rates were determined in COS cells at 37 °C by [^{35}S]methionine pulse-chase labeling in the presence of 1 nM testosterone (Fig. 13). The half-time of degradation of wild-type AR ($t_{½}$ = 1.8 ± 0.3 h) was faster than that of AR V715M ($t_{½}$ = 2.8 ± 0.4 h) and AR H874Y ($t_{½}$ = 3.2 ± 0.4 h) but similar to AR T877A ($t_{½}$ = 2.0 ± 0.5 h). The results indicate that even though all three mutations prolonged the androgen dissociation half-time, only V715M and H874Y increased AR stability in the presence of testosterone.

DISCUSSION

Naturally Occurring Mutations Alter the AR AF2 and Ligand Binding Interface—We have characterized naturally occurring AR mutations in the region of the ligand binding pocket and AF2 binding surface for AR F*XX*LF and coactivator L*XX*LL motifs. The mutations increased or decreased AR functional activity *in vivo* without causing significant changes in equilibrium androgen binding affinity. Germ line mutations in AF2 that cause a phenotypic spectrum of AIS increased the androgen dissociation rate and decreased AR F*XX*LF and SRC/p160 coactivator L*XX*LL motif binding to AF2. Conversely, three AR somatic mutations in prostate cancer slowed the dissociation rate of R1881 by 2-fold and testosterone by up to 4.5-fold. Slower androgen dissociation by the prostate cancer mutants was associated with increased AR transcriptional activity, and for AR V715M and H874Y with increased F*XX*LF and L*XX*LL motif binding to AF2. The location and effect of AIS mutation V889M on ligand dissociation suggest a hormone gateway at the base of AF2 helix 12 between helices 3, 6, 10, and 12, where Val-889 serves as gatekeeper. Moreover, the effects of the AIS and prostate cancer mutations implicate Trp-741 as a critical residue in a structural interplay between AF2, bound ligand, and residues neighboring the ligand.

FXXLF and LXXLL Motif Binding to AF2—The AF2 site in steroid receptors is a hydrophobic surface in the ligand binding domain required for hormone-dependent SRC/p160 coactivator L*XX*LL motif binding (4, 5). AR AF2 has a higher affinity for the AR NH_2-terminal F*XX*LF motif than the coactivator L*XX*LL motifs (13). Differences in the apparent relative AR binding affinities for these helical motifs are attributed in part to flanking residues that interfere with motif binding depending on peptide length (4, 36, 37).

Structural studies have shown subtle induced fit differences between the AR AF2 binding surfaces with bound F*XX*LF and L*XX*LL peptides (13). The $i + 1$ motif side chains contact nearly the same side chains in AF2, as do the $i + 5$ side chains, even with the ~2-Å shift in relative position of the two bound peptides. It was therefore not unexpected that AR mutations in AIS and prostate cancer studied here had similar effects on the two motifs, *i.e.* AIS mutations decreased F*XX*LF and L*XX*LL binding, and two of the prostate cancer mutations increased binding of these motifs.

Despite similarities in the AF2 binding surface, it is F*XX*LF motif binding that slows androgen dissociation (18). This is evident by the ~3 times faster androgen dissociation rate of AR-(507–919) compared with full-length AR. AR-(507–919) retains high affinity equilibrium androgen binding but lacks the AR NH_2-terminal region and thus lacks an N/C interaction. Disrupting the AR N/C interaction by mutations in the NH_2-terminal F*XX*LF motif (14) or F*XX*LF motif binding of melanoma antigen gene protein MAGE-11 (36) also increases intracellular androgen dissociation.

The inability of coactivator L*XX*LL motif binding to slow androgen dissociation from AR was evident in previous studies where TIF2 and AR were coexpressed (14) and from the TIF2-AR chimera studies reported here. TIF2-AR chimeras with wild-type AR ligand binding domain had androgen dissociation rates similar to AR-(507–919) and ~2.5 faster than full-length AR. Prostate cancer mutations V715M, H874Y, and T877A slowed androgen dissociation in the chimeras but not in an L*XX*LL motif-dependent manner.

Slower androgen dissociation resulting from F*XX*LF motif binding to AF2 suggests that structural changes are transmitted from AF2 to the ligand binding pocket. However, induced fit conformational changes noted for the side chains of AF2 charge clamp residues Glu-897 and Lys-720, along with Met-734 and Met-894 (13, 38), do not visibly alter the structure of the ligand binding domain core. Clues that Leu-712 and Ile-898 serve as a conduit for transmission of F*XX*LF binding to the ligand binding pocket exist in the ligand dissociation and structural data. Both L712F and I898T in full-length AR and AR-(509–919) increase androgen dissociation. Leu-712 is located 4.0 Å and Ile-898 5.8 Å from the Met-894 sulfur atom in helix 12. The fully engaged charge

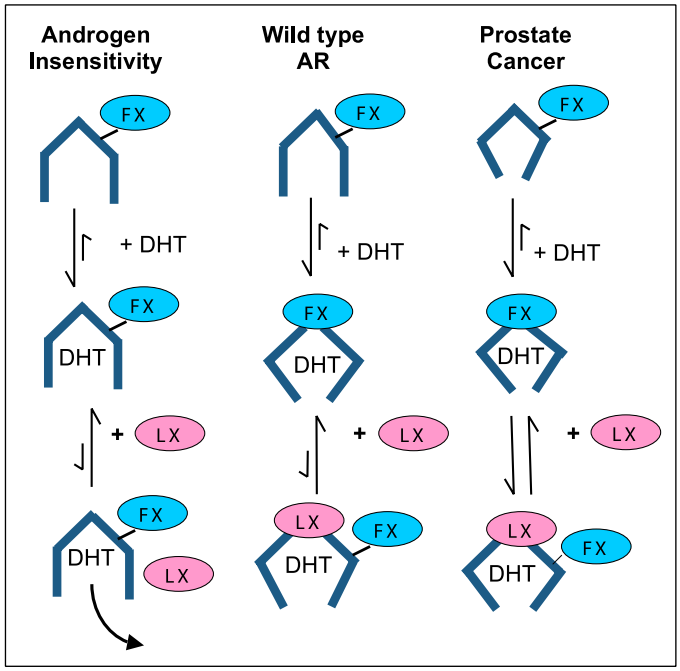

FIGURE 14. **Two-state model of steroid receptor ligand binding and coactivator recruitment.** High affinity agonist binding induces subtle conformational changes in the ligand binding domain that allow for F*XX*LF or L*XX*LL motif binding to AF2. A full agonist effect requires slow ligand dissociation, which is achieved as a result of inherent properties of the ligand (*e.g.* DHT for AR) and is increased by high affinity motif binding to AF2. In the two-state model, high affinity slow dissociating ligands stabilize the active closed state. Faster dissociating ligands that are weaker agonists or antagonists favor the open state. Steroid receptor activity depends on an equilibrium between open and closed states. Naturally occurring AR AF2 mutations impact AR activity *in vivo* by shifting the equilibrium between open and closed states without altering equilibrium agonist binding affinity. AF2 mutations that decrease AR transcriptional activity and cause the androgen insensitivity syndrome (*AIS*) favor the open state, causing more rapid androgen dissociation through effects at the AF2 surface, at the boundary between AF2 and the ligand binding pocket, or more directly at the ligand gateway at the base of AF2 helix 12. In contrast, prostate cancer mutations can increase AR transcriptional activity by favoring the closed state, slowing ligand dissociation and improving F*XX*LF (*FX*) and L*XX*LL (*LX*) motif binding. The effect of AIS and prostate cancer mutations demonstrate ligand-dependent structural communication between AF2 and the ligand binding pocket mediated by subtle changes that the inherent stability of the ligand binding domain. The model suggests steroid receptor activity *in vivo* increases by prolonged retention time of bound ligand.

clamp residues with higher affinity F*XX*LF motif binding may provide a greater stabilizing influence on helix 12 residues such as Met-894 than the more weakly bound L*XX*LL motif that lacks an NH_2-terminal hydrogen bond to charge clamp residue Glu-897 (13, 38). Stabilizing effects passed from helix 12 to Leu-712 and Ile-898 may propagate to Trp-741, which lies above the ligand pocket, resulting in slower ligand dissociation.

In contrast, residues Phe-725, Gln-733, and Ile-737 (group 2) mutated in AIS are situated near Lys-720 in AF2 and $i + 5$ of F*XX*LF and are more remote to the ligand binding pocket. AIS mutations F725L, Q733H, and I737T increase androgen dissociation from full-length AR but not from AR-(507–919), in agreement with two-hybrid assays that the AIS group 2 mutations interfere with F*XX*LF motif binding. Aside from the notable rearrangement of Lys-720, no remarkable structural differences are seen between the $i + 5$ region and the ligand binding pocket when F*XX*LF is bound. This result and their more remote location from the ligand binding pocket suggest that these residues, particularly Phe-725 and Gln-733, stabilize AR primarily by maintaining the bound F*XX*LF motif, which in turn stabilizes the ligand binding core. Residue Ile-737 lies closer to Trp-741 and may more directly influence the ligand binding pocket in response to higher affinity F*XX*LF motif binding. F*XX*LF motif binding also influences the position of the Met-895 side chain that lies close to the steroid D-ring, providing another link in the signal conduit between bound peptide and ligand binding core.

The results from AR and other steroid receptors indicate that motif binding must be high affinity to prolong the half-time of ligand dissociation. The AR F*XX*LF motif peptide binds AF2 with higher affinity than the L*XX*LL motif peptide (13), and it is F*XX*LF motif binding that slows ligand dissociation from AR (14). High affinity coactivator L*XX*LL motif binding to estrogen receptor-α AF2 or in a TIF2-glucocorticoid receptor chimera also slows ligand dissociation (18, 39). This suggests a reciprocal relationship in which ligand binding stabilizes AF2 for motif binding, and high affinity motif binding slows ligand dissociation. The lack of large, defining motif-specific structural differences in the intervening region between AF2 and ligand binding pocket supports the hypothesis that high affinity motif binding imparts subtle stabilizing changes that favor ligand retention, the N/C interaction, coactivator binding, and ultimately receptor activity *in vivo*. Some of the subtle dynamic changes may not be resolved in crystal structures due to rapid kinetics or to the limitations of resolution, precision accuracy in the structure data, and superpositions.

Slow androgen dissociation caused by AR V715M and H874Y in prostate cancer is associated with increased binding of the L*XX*LL and F*XX*LF motifs. T877A, on the other hand, slows androgen dissociation without increasing motif binding. This apparent disconnect for T877A indicates that androgen dissociation slower than that of wild-type AR is not sufficient to increase L*XX*LL motif binding. The structural changes from T877A appear to be limited to the local environment of the ligand binding pocket and are not transmitted to neighboring regions. Similarly, the previously described effects of V730M positioned in AF2 were limited predominantly to the AF2 surface because coactivator L*XX*LL motif binding increased but V730M did not alter androgen dissociation (13). On the other hand, V715M and H874Y are positioned between AF2 and the ligand binding pocket and have bidirectional stabilizing effects on ligand and motif binding. Each of these four mutations increases AR activation in response to the weaker adrenal androgens. Ligand binding domain mutations in prostate cancer can therefore increase AR transcriptional activity through subtle structural changes that favor ligand binding and/or coactivator recruitment.

Structures of the AR ligand binding domain bound to R1881 and F*XX*LF or L*XX*LL motif peptides suggest an induced fit mechanism whereby changes are limited predominantly to side chains in the coactivator binding surface (13). Equilibrium androgen binding affinity was maintained by the AIS and prostate cancer mutants in this study, indicating absence of major structural changes in the interior of the ligand binding domain. We nevertheless observed effects on ligand retention, coactivator recruitment, and receptor activity. A recent computer simulation of the glucocorticoid receptor (GR) investigated the effects of V571M, a residue in GR positioned three residues NH_2-terminal relative to V715M in AR. GR V571M increased transcriptional activity and binding specificity for aldosterone (40). Like V715M and H874Y in AR, V571M is positioned between the coactivator and ligand binding surfaces in GR. The *in silico* molecular dynamic studies of GR V571M predicted changes of less than 0.03 nm, supporting increased coactivator recruitment through subtle structural remodeling in AF2.

A model (Fig. 14) is suggested whereby different functional states of the receptor arise from global changes in structural stability of the ligand binding domain. Ligand binding increases AR stability that is necessary for motif binding to AF2. Receptor activity is augmented by AR mutations such as V715M and H874Y in AF2 and ligand binding boundary region that favor a more stable structural state and slower ligand disso-

ciation and improved AR F*XX*LF or coactivator L*XX*LL motif binding. The active state is achieved by agonist binding and favored by mutations that lend stability through mechanisms such as reduced backbone fluctuations and improved anchoring of helices 3 and 12 as suggested for GR V571M (40). If similar to GR V571M, methionine in the AR prostate cancer mutant V715M might be better accommodated and improve van der Waals interactions that increase overall stability of the ligand binding domain. Increased inherent stability of the ligand binding domain by prostate cancer mutations enhance the AR response to weaker or lower concentrations of androgens. Mutations that decrease structural stability of the ligand binding domain reduce receptor activity in response to circulating androgens and cause AIS. Single amino acid substitutions alter the equilibrium between the active closed state and inactive open state that impacts ligand and coactivator binding and ultimately receptor activity.

Increased Coactivator Recruitment in Prostate Cancer—A number of mechanisms have been proposed to account for AR-mediated increases in cell growth in prostate cancer. These include AR gene amplification (41), increased cross-talk through growth factor signaling pathways (32), increased SRC/p160 coactivator expression (42), and AR mutations. The reported AR mutation rate in prostate cancer varies (43–47) with recent studies suggesting a frequency of ~5% (43, 48–52) that increases in later stages of the disease following androgen withdrawal or anti-androgen therapy (48, 53–55). The low incidence of AR mutations in early stage clinical specimens argues against their role in prostate cancer initiation (54). On the other hand, functional mutations that arise during tumor progression associated with genetic instability suggest positive selection for tumor cell survival (21, 56). Most AR mutants in prostate cancer retain AR transcriptional activity in response to testosterone or DHT, and nearly half the reported mutants are active in response to a range of ligands, including adrenal steroids (21, 25, 28, 52, 57, 58). AR mutations described here can contribute to increased AR functional activity and favor prostate cancer cell survival and expansion through mechanisms that include increased retention time of bound androgen or other steroids, increased SRC/p160 coactivator recruitment, and increased AR stability.

The prostate cancer mutations studied in this report were identified previously in prostate cancer specimens and cell lines (21, 22, 25, 27, 28, 44, 52, 59). T877A occurs in the LNCaP cell line (22, 27) and in multiple specimens of prostate cancer (52). Thr-877 is in the linker region before AF2 helix 12 and in the ligand pocket close to rings C and D of the bound steroid. The T877A mutation increases the space around the steroid D-ring to accommodate other steroids, consistent with the promiscuous ligand binding properties of this mutant (34, 57, 59–62). His-874 in helix 10 is between AF2 and the ligand binding pocket (61, 63) above rings C and D of the bound steroid. H874Y was identified in the CWR22 human prostate cancer xenograft and also displays reduced ligand specificity (21). V715M is in helix 3 at the boundary between AF2 and the steroid A-ring side of the binding pocket and was identified in a poorly differentiated recurrent late stage prostate cancer (25).

The similar effects of H874Y and V715M on androgen dissociation and F*XX*LF and L*XX*LL motif binding may result from different structural influences. H874Y would displace a conserved structural water shown in Fig. 12, which might allow direct hydrogen bonding to the helix 5 backbone. V715M may increase hydrophobic interactions to stabilize ligand binding. It is noteworthy that 6 other methionine residues reside directly in the ligand binding pocket and that His-874 and Val-715 are on opposite sides of AF2, each within ~5 Å of Trp-741, a hydrophobic residue that contacts the ligand and has a role in retaining ligand (10). H874Y and V715M introduce extended hydrophobic side chains that improve interactions with Trp-741 that may prolong ligand retention time by stabilizing Trp-741 and optimizing contacts between Trp-741 and the ligand. T877A also lies ~5 Å from Trp-741. The surprisingly well compensated alanine substitution of T877A forfeits a hydrogen bond to the D-ring of testosterone and DHT (34, 64), supporting the importance of hydrophobic interactions in stabilizing bound ligand. Interactions between Trp-741 and bound ligand may have a role in establishing the DHT and testosterone dissociation rates from wild-type AR.

Prostate cancers are initially androgen-dependent, regress after androgen deprivation therapy, and resume growth after a period of remission despite low circulating androgen (48, 49, 65). AR is expressed in most recurrent prostate cancers (66) and likely contributes to recurrent tumor growth (67, 68). Recent studies have shown DHT levels decline in recurrent prostate cancer tissue following androgen deprivation therapy, whereas testosterone persists at tissue levels similar to benign prostatic hyperplasia (69). AR mutations that slow dissociation of testosterone or weaker adrenal androgens may stabilize the ligand binding domain and facilitate growth of recurrent prostate cancer through AR mechanisms in concert with enhanced mitogen signaling.

Why DHT Is a More Potent Androgen than Testosterone—Our characterization of AIS and prostate cancer AR mutants indicates a functional link between androgen dissociation rate and AR activity that parallels the known physiological potencies of testosterone and DHT. AR binds these two biologically active androgens with similar equilibrium binding affinity (K_d) determined from the ratio of association and dissociation rate constants (31). Yet testosterone dissociates ~3 times faster than DHT. Dissociation of both androgens is slowed by the AR N/C interaction mediated by F*XX*LF motif binding to AF2, which decreases AR degradation and increases androgen-dependent gene activation (11, 16). The importance of prolonged ligand retention for steroid receptor activity is also applicable to estrogen receptor-α, which binds estriol and 17β-estradiol with similar high affinity, but like the relationship between testosterone and DHT, estriol dissociates more rapidly and is a weaker estrogen than 17β-estradiol (70). More recent evidence indicates that removal of the ligand-bound estrogen receptor-α from chromatin through degradation in a transcription-coupled manner is another important mechanism of transcriptional control (71, 72).

A full or amplified agonist response mediated by AR and perhaps other steroid receptors appears to depend on sufficient ligand retention time to maintain structural stability in the ligand binding domain. The human 5α-reductase deficiency syndrome indicates that DHT is required for AR functional activity during embryonic development. Naturally occurring mutations in the human 5α-reductase type 2 gene reduce the conversion of testosterone to DHT, cause ambiguous external sex phenotypes, and reduce prostate size in 46,XY genetic males (73). AR mutations in prostate cancer can slow the dissociation of testosterone to a rate similar to that of DHT, which increases AR stability and transcriptional activity in response to testosterone or other weaker androgens in this disease. Ligand retention time as a key determinant of AR functional activity is supported by the rapid dissociation rates of high affinity AR antagonists (35).

Requirements for AR Stabilization—Most steroid receptors are degraded subsequent to agonist-induced gene activation, presumably as a feedback mechanism to limit the hormone response. AR appears an exception because it is degraded more slowly in the presence of bound androgen (74), and stabilization is linked to increased transcriptional activity *in vivo*. AR degradation increases in response to mutations that increase androgen dissociation and cause AIS (20). Conversely, AR

mutations in prostate cancer can further slow androgen dissociation, stabilize AR, and contribute to increased androgen-dependent and -independent AR activity in prostate cancer. The cancer-testis protein MAGE-11 selectively binds the AR NH_2-terminal F*XX*LF motif and competes for the AR N/C interaction. Binding of MAGE-11 relieves the competitive inhibition of SRC/p160 coactivator L*XX*LL motif binding to AF2 caused by AR F*XX*LF motif binding in the N/C interaction, thereby increasing androgen dissociation and AR turnover. As a result, AR functional activity increases by way of greater SRC/p160 coactivator recruitment (36).

A number of mechanisms involving increased SRC/p160 coactivator recruitment appear to contribute to greater AR activity in clinically recurrent prostate cancer. These include increased expression levels of TIF2 and SRC1 (42) and a broader spectrum of active androgens resulting from mutations like T877A (21, 27) and H874Y (21, 26) and mutations such as V730M that increase coactivator L*XX*LL motif binding without altering the androgen dissociation rate (13). Here we report that AR mutations can provide inherent structural stability to the ligand binding domain, slow androgen dissociation, and improve SRC/p160 coactivator recruitment. SRC/p160 coactivator binding increases receptor-mediated gene activation through the recruitment of CBP/p300 and PCAF for histone acetylation and chromatin remodeling.

Acknowledgment—We thank K. Michelle Cobb for excellent technical assistance.

REFERENCES

1. Glass, C. K., and Rosenfeld, M. G. (2000) *Gene Dev.* **14,** 121–141
2. Simental, J. A., Sar, M., Lane, M. V., French, F. S., and Wilson, E. M. (1991) *J. Biol. Chem.* **266,** 510–518
3. He, B., Bai, S., Hnat, A. T., Kalman, R. I., Minges, J. T., Patterson, C., and Wilson, E. M. (2004) *J. Biol. Chem.* **279,** 30643–30653
4. He, B., and Wilson, E. M. (2003) *Mol. Cell. Biol.* **23,** 2135–2150
5. Darimont, B. D., Wagner, R. L., Apriletti, J. W., Stallcup, M. R., Kushner, P. J., Baxter, J. D., Fletterick, R. J., and Yamamoto, K. R. (1998) *Genes Dev.* **12,** 3343–3356
6. Feng, W., Ribeiro, R. C., Wagner, R. L., Nguyen, H., Apriletti, J. W., Fletterick, R. J., Baxter, J. D., Kushner, P. J., and West, B. L. (1998) *Science* **280,** 1747–1749
7. Moras, D., and Gronemeyer, H. (1998) *Curr. Opin. Cell Biol.* **10,** 384–391
8. Gottlieb, B., Beitel, L. K., Wu, J. H., and Trifiro, M. (2004) *Hum. Mutat.* **23,** 527–533
9. Quigley, C. A., De Bellis, A., Marschke, K. B., El-Awady, M. K., Wilson, E. M., and French, F. S. (1995) *Endocr. Rev.* **16,** 271–321
10. He, B., Kemppainen, J. A., Voegel, J. J., Gronemeyer, H., and Wilson, E. M. (1999) *J. Biol. Chem.* **274,** 37219–37225
11. Langley, E., Kemppainen, J. A., and Wilson, E. M. (1998) *J. Biol. Chem.* **273,** 92–101
12. Spencer, T. E., Jenster, G., Burcin, M. M., Allis, C. D., Zhou, J., Mizzen, C. A., McKenna, N. J., Onate, S. A., Tsai, S. Y., Tsai, M. J., and O'Malley, B. W. (1997) *Nature* **389,** 194–198
13. He, B., Gampe, R. T., Kole, A. J., Hnat, A. T., Stanley, T. B., An, G., Stewart, E. L., Kalman, R. I., Minges, J. T., and Wilson, E. M. (2004) *Mol. Cell* **16,** 425–438
14. He, B., Kemppainen, J. A., and Wilson, E. M. (2000) *J. Biol. Chem.* **275,** 22986–22994
15. Langley, E., Zhou, Z. X., and Wilson, E. M. (1995) *J. Biol. Chem.* **270,** 29983–29990
16. He, B., Lee, L. W., Minges, J. T., and Wilson, E. M. (2002) *J. Biol. Chem.* **277,** 25631–25639
17. He, B., and Wilson, E. M. (2002) *Mol. Gen. Metab.* **75,** 293–298
18. He, B., Bowen, N. T., Minges, J. T., and Wilson, E. M. (2001) *J. Biol. Chem.* **276,** 42293–42301
19. Quigley, C. A., Tan, J. A., He, B., Zhou, Z. X., Mebarki, F., Morel, Y., Forest, M., Chatelain, P., Ritzen, E. M., French, F. S., and Wilson, E. M. (2004) *Mech. Ageing Dev.* **125,** 683–695
20. Zhou, Z. X., Lane, M. V., Kemppainen, J. A., French, F. S., and Wilson, E. M. (1995) *Mol. Endocrinol.* **9,** 208–218
21. Tan, J., Sharief, Y., Hamil, K. G., Gregory, C. W., Zang, D. Y., Sar, M., Gumerlock, P. H., DeVere White, R. W., Pretlow, T. G., Harris, S. E., Wilson, E. M., Mohler, J. L., and French, F. S. (1997) *Mol. Endocrinol.* **11,** 450–459
22. Harris, S. E., Harris, M. A., Rong, Z., Hall, J., Judge, S., French, F. S., Joseph, D. R., Lubahn, D. B., Simental, J. A., and Wilson, E. M. (1991) in *Molecular and Cellular Biology of Prostate Cancer* (Karr, J. P., Coffey, D. S., Smith, R. G., and Tindall, D. J., eds) pp. 315–330, Plenum Publishing Corp., New York
23. Voegel, J. J., Heine, M. J., Tini, M., Vivat, V., Chambon, P., and Gronemeyer, H. (1998) *EMBO J.* **17,** 507–519
24. Feldman, B. J., and Feldman, D. (2001) *Nat. Rev. Cancer* **1,** 34–45
25. Culig, Z., Hobisch, A., Cronauer, M. V., Cato, A. C., Hittmair, A., Radmayr, C., Eberle, J., Bartsch, G., and Klocker, H. (1993) *Mol. Endocrinol.* **7,** 1541–1550
26. Duff, J., and McEwan, I. J. (2005) *Mol. Endocrinol.* **19,** 2943–2954
27. Veldscholte, J., Ris-Stalpers, C., Kuiper, G. G., Jenster, G., Berrevoets, C., Claassen, E., van Rooij, H. C., Trapman, J., Brinkmann, A. O., and Mulder, E. (1990) *Biochem. Biophys. Res. Commun.* **173,** 534–540
28. Peterziel, H., Culig, Z., Stober, J., Hobisch, A., Radmayr, C., Bartsch, G., Klocker, H., and Cato, A. C. (1995) *Int. J. Cancer* **63,** 544–550
29. Mononen, N., Syrjakoski, K., Matikainen, M., Tammela, T. L., Schleutker, J., Kallioniemi, O. P., Trapman, J., and Koivisto, P. A. (2000) *Cancer Res.* **60,** 6479–6481
30. Gruber, S. B., Chen, H., Tomsho, L. P., Lee, N., Perrone, E. E., and Cooney, K. A. (2003) *Prostate* **54,** 306–309
31. Wilson, E. M., and French, F. S. (1976) *J. Biol. Chem.* **251,** 5620–5629
32. Gregory, C. W., Fei, X., Ponguta, L. A., He, B., Bill, H. M., French, F. S., and Wilson, E. M. (2004) *J. Biol. Chem.* **279,** 7119–7130
33. Needham, M., Raines, S., McPheat, J., Stacey, C., Ellston, J., Hoare, S., and Parker, M. (2000) *J. Steroid Biochem. Mol. Biol.* **72,** 35–46
34. Sack, J. S., Kish, K. F., Wang, C., Attar, R. M., Kiefer, S. E., An, Y., Wu, G. Y., Scheffler, J. E., Salvati, M. E., Krystek, S. R., Weinmann, R., and Einspahr, H. M. (2001) *Proc. Natl. Acad. Sci. U. S. A.* **98,** 4904–4909
35. Kemppainen, J. A., Langley, E., Wong, C. I., Bobseine, K., Kelce, W. R., and Wilson, E. M. (1999) *Mol. Endocrinol.* **13,** 440–454
36. Bai, S., He, B., and Wilson, E. M. (2005) *Mol. Cell. Biol.* **25,** 1238–1257
37. Estebanez-Perpina, E., Moore, J. M., Mar, E., Delgado-Rodrigues, E., Nguyen, P., Baxter, J. D., Buehrer, B. M., Webb, P., Fletterick, R. J., and Guy, R. K. (2005) *J. Biol. Chem.* **280,** 8060–8068
38. Hur, E., Pfaff, S. J., Payne, E. S., Gron, H., Buehrer, B. M., and Fletterick, R. J. (2004) *PLoS Biol.* **2,** 1303–1312
39. Gee, A. C., Carlson, K. E., Martini, P. G., Katzenellenbogen, B. S., and Katzenellenbogen, J. A. (1999) *Mol. Endocrinol.* **13,** 1912–1923
40. Carlsson, P., Koehler, K. F., and Nilsson, L. (2005) *Mol. Endocrinol.* **19,** 1960–1977
41. Koivisto, P., Hyytinen, E., Palmberg, C., Tammela, T., Visakorpi, T., Isola, J., and Kallioniemi, O. P. (1995) *Am. J. Pathol.* **147,** 1608–1614
42. Gregory, C. W., He, B., Johnson, R. T., Ford, O. H., Mohler, J. L., French, F. S., and Wilson, E. M. (2001) *Cancer Res.* **61,** 4315–4319
43. Newmark, J. R., Hardy, D. O., Tonb, D. C., Carter, B. S., Epstein, J. I., Isaacs, W. B., Brown, T. R., and Barrack, E. R. (1992) *Proc. Natl. Acad. Sci. U. S. A.* **89,** 6319–6323
44. Taplin, M. E., Bubley, G. J., Shuster, T. D., Frantz, M. E., Spooner, A. E., Ogata, G. K., Keer, H. N., and Balk, S. P. (1995) *N. Engl. J. Med.* **332,** 1393–1398
45. Taplin, M. E., and Ho, S. M. (2001) *J. Clin. Endocrinol. Metab.* **86,** 3467–3477
46. Terouanne, B., Nirde, P., Rabenoelina, F., Bourguet, W., Sultan, C., and Auzou, G. (2003) *Mol. Pharmacol.* **63,** 791–798
47. Tilley, W. D., Buchanan, G., Hickey, T. E., and Bentel, J. M. (1996) *Clin. Cancer Res.* **2,** 277–285
48. Balk, S. P. (2002) *Urology* **60,** 132–138
49. Gelmann, E. P. (2002) *J. Clin. Oncol.* **20,** 3001–3015
50. Heinlein, C. A., and Chang, C. (2004) *Endocr. Rev.* **25,** 276–308
51. Koivisto, P., Kolmer, M., Visakorpi, T., and Kallioniemi, O. P. (1998) *Am. J. Pathol.* **152,** 1–9
52. Shi, X. B., Ma, A. H., Xia, L., Kung, H. J., and de Vere White, R. W. (2002) *Cancer Res.* **62,** 1496–1502
53. Hara, T., Miyazaki, J., Araki, H., Yamaoka, M., Kanzaki, N., Kusaka, M., and Miyamoto, M. (2003) *Cancer Res.* **63,** 149–153
54. Marcelli, M., Ittmann, M., Mariani, S., Sutherland, R., Nigam, R., Murthy, L., Zhao, Y., DiConcini, D., Puxeddu, E., Esen, A., Eastham, J., Weigel, N. L., and Lamb, D. J. (2000) *Cancer Res.* **60,** 944–949
55. Taplin, M. E., Bubley, G. J., Ko, K. J., Small, E. J., Upton, M., Rajeshkumar, B., and Balk, S. P. (1999) *Cancer Res.* **59,** 2511–2515
56. Lengauer, C., Kinzler, K. W., and Vogelstein, B. (1998) *Nature* **396,** 643–649
57. Chang, C. Y., Walther, P. J., and McDonnell, D. P. (2001) *Cancer Res.* **61,** 8712–8717
58. Elo, J. P., Kvist, L., Leinonen, K., Isomaa, V., Henttu, P., Lukkarinen, O., and Vihko, P. (1995) *J. Clin. Endocrinol. Metab.* **80,** 3494–3500
59. Matias, P. M., Carrondo, M. A., Coelho, R., Thomaz, M., Zhao, X. Y., Wegg, A., Crusius, K., Egner, U., and Donner, P. (2002) *J. Med. Chem.* **45,** 1439–1446
60. Krishnan, A. V., Zhao, X. Y., Swami, S., Brive, L., Peehl, D. M., Ely, K. R., and Feldman, D. (2002) *Endocrinology* **143,** 1889–1900
61. Steketee, K., Timmerman, L., Ziel-van der Made, A. C., Doesburg, P., Brinkmann, A. O., and Trapman, J. (2002) *Int. J. Cancer* **100,** 309–317
62. Zhao, X. Y., Malloy, P. J., Krishnan, A. V., Swami, S., Navone, N. M., Peehl, D. M., and Feldman, D. (2000) *Nat. Med.* **6,** 703–706
63. McDonald, S., Brive, L., Agus, D. B., Scher, H. I., and Ely, K. R. (2000) *Cancer Res.* **60,** 2317–2322

64. Matias, P. M., Donner, P., Coelho, R., Thomaz, M., Peixoto, C., Macedo, S., Otto, N., Joschko, S., Scholz, P., Wegg, A., Basler, S., Schafer, M., Egner, U., and Carrondo, M. A. (2000) *J. Biol. Chem.* **275,** 26164–26171
65. Aquilina, J. W., Lipsky, J. J., and Bostwick, D. G. (1997) *J. Natl. Cancer Inst.* **89,** 689–695
66. van der Kwast, T. H., Schalken, J., Ruizeveld de Winter, J. A., van Vroonhoven, C. C. J., Mulder, E., Boersma, W., and Trapman, J. (1991) *Int. J. Cancer* **48,** 189–193
67. Gregory, C. W., Hamil, K. G., Kim, D., Hall, S. H., Pretlow, T. G., Mohler, J. L., and French, F. S. (1998) *Cancer Res.* **58,** 5718–5724
68. Zegarra-Moro, O. L., Schmidt, L. J., Huang, H., and Tindall, D. J. (2002) *Cancer Res.* **62,** 1008–1013
69. Mohler, J. L., Gregory, C. W., Ford, O. H., Kim, D., Weaver, C. M., Petrusz, P., Wilson, E. M., and French, F. S. (2004) *Clin. Cancer Res.* **10,** 440–448
70. Anderson, J. N., Peck, E. J., and Clark, J. H. (1975) *Endocrinology* **96,** 160–167
71. Shang, Y., Hu, X., DiRenzo, J., Lazar, M. A., and Brown, M. (2000) *Cell* **103,** 843–852
72. Lonard, D. M., Nawaz, Z., Smith, C. L., and O'Malley, B. W. (2000) *Mol. Cell* **5,** 939–948
73. Imperato-McGinley, J., Guerrerro, J. L., Gautier, T., and Peterson, R. E. (1974) *Science* **186,** 1213–1215
74. Kemppainen, J. A., Lane, M. V., Sar, M., and Wilson, E. M. (1992) *J. Biol. Chem.* **267,** 968–974
75. Bohl, C. E., Miller, D. D., Chen, J., Bell, C. E., and Dalton, J. T. (2005) *J. Biol. Chem.* **280,** 37747–37754
76. Georget, V., Terouanne, B., Lumbroso, S., Nicolas, J. C., and Sultan, C. (1998) *J. Clin. Endocrinol. Metab.* **83,** 3597–3603
77. Nakao, R., Yanase, T., Sakai, Y., Haji, M., and Nawata, H. (1993) *J. Clin. Endocrinol. Metab.* **77,** 103–107
78. Poujol, N., Lumbroso, S., Terouanne, B., Lobaccaro, J. M., Bourguet, W., and Sultan, C. (2002) *J. Clin. Endocrinol. Metab.* **87,** 5793–5800
79. Hiort, O., Huang, Q., Sinnecker, G. H., Sadeghi-Nejad, A., Kruse, K., Wolfe, H. J., and Yandell, D. W. (1993) *J. Clin. Endocrinol. Metab.* **77,** 262–266
80. Hiort, O., Sinnecker, G. H., Holterhus, P. M., Nitsche, E. M., and Kruse, K. (1998) *J. Pediatr.* **132,** 939–943
81. Holterhus, P. M., Sinnecker, G. H., and Hiort, O. (2000) *J. Clin. Endocrinol. Metab.* **85,** 3245–3250
82. Ahmed, S. F., Cheng, A., Dovey, L., Hawkins, J. R., Martin, H., Rowland, J., Shimura, N., Tait, A. D., and Hughes, I. A. (2000) *J. Clin. Endocrinol. Metab.* **85,** 658–665
83. De Bellis, A., Quigley, C. A., Marschke, K. B., El-Awady, M. K., Lane, M. V., Smith, E. P., Sar, M., Wilson, E. M., and French, F. S. (1994) *J. Clin. Endocrinol. Metab.* **78,** 513–522
84. Essawi, M., Gad, Y. Z., El-Rouby, O., Temtamy, S. A., Sabour, Y. A., and El-Awady, M. K. (1997) *Dis. Markers* **13,** 99–105
85. MacLean, H. E., Ball, E. M., Rekaris, G., Warne, G. L., and Zajac, J. D. (2004) *Hum. Mutat.* **23,** 287
86. Pinsky, L., Trifiro, M., Kaufman, M., Beitel, L. K., Mhatre, A., Kazemi-Esfarjani, P., Sabbaghian, N., Lumbroso, R., Alvarado, C., Vasiliou, M., and Gottlieb, B. (1992) *Clin. Investig. Med.* **15,** 456–472